Modelling Internal Solitary Waves and the Alternative Ostrovsky Equation

by

Yangxin He

A thesis
presented to the University of Waterloo
in fulfillment of the
thesis requirement for the degree of
Master of Mathematics
in
Applied Mathematics

Waterloo, Ontario, Canada, 2014

© Yangxin He 2014

I hereby declare that I am the sole author of this thesis. This is a true copy of the thesis, including any required final revisions, as accepted by my examiners.

I understand that my thesis may be made electronically available to the public.

Abstract

Internal solitary waves (ISWs) are commonly observed in the ocean, and they play important roles in many ways, such as transport of mass and various nutrients through propagation. The fluids considered in this thesis are assumed to be incompressible, inviscid, non-diffusive and to be weakly affected by the Earth's rotation. Comparisons of the evolution of an initial solitary wave predicted by a fully nonlinear model, IGW, and two weakly-nonlinear wave equations, the Ostrovsky equation and a new alternative Ostrovsky equation, are done.

Resolution tests have been run for each of the models to confirm that the current choices of the spatial and time steps are appropriate. Then we have run three numerical simulations with varying initial wave amplitudes. The rigid-lid approximation has been used for all of the models. Stratification, flat bottom and water depth stay the same for all three simulations.

In the simulation analysis, we use the results from the IGW as the standard. Both of the two weakly nonlinear models give fairly good predictions regarding the leading wave amplitudes, shapes of the wave train and the propagation speeds. However, the weakly nonlinear models over-predict the propagation speed of the leading solitary wave and that the alternative Ostrovsky equation gives the worst prediction. The difference between the two weakly nonlinear models decreases as the initial wave amplitude decreases.

Acknowledgements

I would like to take this opportunity to thank my supervisor, Professor Kevin Lamb, for his patient guidance and support. This thesis would not have been completed without him.

I would also like to thank Professors Marek Stastna and Francis Poulin for being my defense committee and reading my thesis, especially in providing constructive feedback and correcting my awkward sentences.

Many thanks to Anson for standing by me and making my life special.

Dedication

To my mom.

Contents

List of Tables

List of Figures

Chapter 1

Introduction

1.1 Observations and Importance of Internal Waves

Internal waves (IWs) are waves that propagate in the interior of a density stratified fluid under the influence of gravitational restoring forces. For example, these waves can be seen from the visible oscillations in two-layer immiscible colored fluids of different density in a transparent plastic box. The occurrence of this wave is due to the different densities of the two fluids, especially the discrete density change across the interface. The larger the density difference the larger the wave frequency for a given wavelength.

The common occurrence of solitary waves in the ocean has been widely accepted. John Scott Russell (1838, 1844) seemed to be the first one who documented the observation of surface solitary waves in the shallow water of the Union canal in Scotland. Following Russell, some other observations of solitary waves were made by Wallace (1869). The solitary wave solutions of the surface waves were found in 1871 and 1876, and the KdV equation was derived in 1895. More details of the solitons will be mentioned later in the next subsection. Some later observations of solitary waves include Fu and Holt (1982), Apel and Gonzales (1984), Apel et al. (1985) and Liu et al. (1985). In 1965, Perry & Schimke's measurements detected groups of internal waves up to 80m high and 2000m long in the Andaman Sea. Due to the development of the ocean instrumentation and remote sensors, many significant observations were made in the 1970s, such as, Halpern (1971) in Massachusetts Bay, Thorpe (1971) and Hunkins & Fliegel (1973) in Loch Ness and Seneca Lake, New York. Meanwhile, Ziegenbein (1969, 1970) made similar observations in the Strait of Gibraltar, which provided clear evidence of the ISWs. Apel et al. (1975) reported the occurrence of internal solitray waves (ISWs) in the New York Bight based on the collective data in 1972 and 1973. More examples about the observations of ISWs can be found in the second edition of the *Atlas of Oceanic Internal Solitary Waves*, where around 300 cases from 54

regions over the world are listed.

There are two terms for large nonlinear isolated IWs that are often used, internal solitary waves (ISWs) and solitons. ISWs are a class of isolated nonlinear waves. A soliton is an internal solitary wave, which will retain its shape and velocity after colliding with any other waves. As will be seen later, the solitary wave solutions of KdV equations are solitons. The ISWs in the ocean are approximately solitons but strictly speaking they are not.

There are various ways to generate ISWs, one of which is through tide-topography interactions. When tidal current flows over an irregular seabed, the varying seabed features will cause vertical motion generating internal waves. If the generated waves are large enough, as they propagate away, the initial shape may start to steepen and evolve into nonlinear internal waves. As a result of this process, ISWs are commonly observed in stratified coastal regions. However, the actual process may be more complicated than a mere tide-topography interaction. For example, the nonlinear internal waves can be trapped inside the baroclinic tidal flows as they propagate together, where they form a fixed phase relationship. ([27])

ISWs are important for many reasons. The propagation of ISWs can last up to several hundred kilometers with the transport of both mass and momentum. They can also impose large stresses on offshore oil-drilling rigs, which is one of the reasons to study them in the early times ([44]). The propagation of ISWs causes large amount of velocity shear and leads to turbulence and mixing. This usually brings various nutrients from the seabed into the water column. As a result, the circulation of the nutrients provides fertilization to the local region and the biology system.

Observations show that a number of peculiarities associated with IWs can only be explained by the nonlinear theory [Garrett & Munk 1979; Morozov 1985]. Great advances in the nonlinear wave theories have been achieved since the 1970s. Various weakly nonlinear and fully nonlinear equations are derived to model the evolutions of ISWs. Both models have their advantages and restrictions.

1.2 Wave Models

1.2.1 Weakly Nonlinear Models

Weakly nonlinear models are derived for waves whose amplitudes are small compared with the water depth. Probably the most basic and widely used model for describing ISW dy-

namics is the Korteweg-de Vries (KdV) equation. The history of the KdV equation began with John Russell's experiment in 1834, followed by Boussinesq and Rayleigh, who found the solitary wave solution independently in 1871 and 1876. Then in 1895, Diederik Korteweg and his student Gustav de Vries derived the KdV equation, which describes weakly nonlinear, long and unidirectional surface water waves. Followed by this original work, Zabusky & Kruskal (1965) discovered the soliton solution, and later a cubic nonlinear term was added to incorporate higher-order nonlinear effects. This equation is known as eKdV or Gardner equation, which can deal with waves of larger amplitudes compared with the classic KdV equation. When applied to the internal solitons, KdV type theories provide quite satisfactory results as well, even though there are many other solitary wave equations derived after this. Other weakly nonlinear internal wave theories for different scales include, a model developed by Benjamin (1967) and Ono (1975) for infinitely deep fluids, and a model derived by Joseph (1977) and Kubota et al. (1978) for intermediate depth.

Maxworthy (1983) pointed out that in some instances the effects of the Earths rotation cannot be ignored. The effects of rotation may be comparable to weak nonlinear and dispersive effects. Ostrovsky (1978) firstly extended the unidirectional KdV equation to include the effects of weak rotation on nonlinear dispersive internal waves. The resulting equation is known as the Ostrovsky equation and many conservation laws have been derived from it. There are no solitary wave solutions of the Ostrovsky equation. If we use solitary solutions of the KdV as the initial condition for the Ostrovsky equation, the solitary wave will decay in time and its energy will slowly be diverted to an inertia-gravity wave train due to rotational effects. Numerical studies of the Ostrovsky equation have shown an interesting phenomenon: the wave train can steepen up and form a second solitary-like wave behind the leading solitary wave. This second solitary-like wave can then decay and this whole process may repeat and lead to more solitary-like waves in the wave train ([48]). Modeling ISWs with weak rotational effects is the focus of this thesis.

Many simulations have been run to model internal waves with rotational effects. Holloway & Pelinovsky & Talipova (1999) used the Gardner-Ostrovsky equation with a dissipation term to model evolutions of the shoaling internal tides observed on the north west shelf (NWS) of Australia. Numerical results were compared with the observations on the NWS. The paper shows that rotation is important for modeling internal waves even for low latitude regions. Helfrich (2007) used a fully nonlinear, weakly nonhydrostatic theory, i.e. MCC theory, to model the propagation of ISWs. Grimshaw & Pelinovsky & Stepanyants & Talipova (2006) used the Gardner-Ostrovsky equation to model ISWs on the NWS. Both depth variation and horizontal variability of the stratification were considered in the model. Johnson & Grimshaw (2013) and Grimshaw & Helfrich & Johnson (2012) used a reduced modified Ostrovsky equation, where the linear dispersive term and the quadratic term have been set to 0, to determine the constraint for wave breaking. They show that the

reduced Ostrovsky equation is integrable given certain slope constraints. Here, equations with an infinite number of integrals of motion in involution are called integrable. ([1]) Wave breaking can occur if the constraint is not satisfied. Grimshaw & Helfrich (2008) ran a long-time numerical simulation of the Ostrovsky equation to show that a localized wave packet emerged as a persistent feature.

Since ISWs are usually observed around varying or steep topography in the ocean, such as coastal regions, recently various of KdV-type equations have been developed to incorporate the effects of shoaling. As such, the coefficients of the KdV equations change with the varying topography. Lamb (2002, 2003) simulated behaviors of waves shoaling over changing topography, and then further explored the relations of the configuration of the shoaling waves and the limiting form of the corresponding solitary waves. There will not be any trapped cores if the limiting form of the ISWs includes a conjugate flow. Here, a conjugate flow refers to the horizontally uniform flow that is in the center of long flat waves [Benjamin (1996); Mehrotra & Kelly (1973); Lamb & Wan 1998]. Grue el al. (2000) found that a core can be formed if the limiting form corresponds to the maximum horizontal velocity in the wave matching the wave speed. However, this thesis only considers waves propagating on a flat bottom and all the coefficients of the KdV theories are constant through space and time.

There are other extensions of the KdV equations. The KdV equation can be extended to account for weak two-dimensionality, i.e., two horizontal dimensions x and y with a vertical scale z. The resulting equation is called the Kadomtsev and Petviashvili (1970, KP) equation. Pierini (1989) used the KP equation to simulate the waves in the Strait of Gibraltar, and the implementation was done by Chen and Liu (1995).

Laboratory experiments have been conducted to investigate and compare the validity of weakly nonlinear models. Koop & Butler (1981) and Segur & Hammack (1982) showed that KdV performs quantitatively better than the Benjamin-Ono equation, for weakly nonlinear waves in deep water. Through some two-layer fluid experiment with $\frac{h_1}{h_2} = 0.24$, Grue et al. (1999) showed that KdV theory can model wave with amplitudes up to $\frac{\eta_0}{h_1} \approx 0.4$, but it does not manage to capture the broadening of ISWs with increasing amplitudes. Michallet & Barthelemy (1998) noticed improvements from eKdV. In their two-layer experiment for $0.4 < \frac{h_1}{h_1+h_2} < 0.6$, prediction of eKdV equation matches excellent with the lab results.

1.2.2 Fully Nonlinear Models

In contrast with the weakly nonlinear models, fully nonlinear models make fewer simplifications, thus they are a more accurate set of equations. As a result, there are no restrictions when applying the fully nonlinear models. For example, the wave amplitude

does not need to be small as that in the KdV-type equations. Fully nonlinear models show better results than the weakly nonlinear models as well. However, the disadvantages are that solving these models are usually more time-consuming and expensive ([17]). Hence, it is very important to develop and improve weakly nonlinear models so that they can produce comparable results as the fully nonlinear models do, while being more efficient and cheaper. However, we can only expect the weakly nonlinear models to perform well within a restricted set of phenomena, since they have many limitations and each weakly nonlinear equation has its validity range.

Laboratory experiments have also been conducted to check the fully nonlinear model. For example, Michallet & Barthelemy (1998) and Grue et al. (1999) found nice agreement of the fully nonlinear two-layer model and their laboratory measurements of an ISW over a broad range of relative layer depths.

1.3 Thesis Structure and Goals

Some brief background information about the fully nonlinear equations with Earth's rotation will be mentioned in Chapter 2. Derivations and solution analysis of the weakly nonlinear equations, i.e., the alternative Ostrovsky equation, the Ostrovsky equation and KdV-type equations, will be covered in Chapter 3. Numerical models and the corresponding simulation results will be illustrated in Chapter 4 and 5. Conclusions and summary will be in the last chapter.

A new equation, i.e., the alternative Ostrovsky equation, has been introduced. The goal of this thesis is to compare this new equation with the existing Ostrovsky equation, and further compare them with the fully nonlinear model through numerical simulations.

Chapter 2

Theoretical Background

2.1 Fully Nonlinear Equations with Rotation

This thesis considers a fluid that is stratified, incompressible, inviscid and non-diffusive, moving in a rotating-reference frame. The momentum equations, as a result of Newton's second law, are

$$\rho(\frac{D\vec{U}}{Dt} + 2\vec{\Omega} \times \vec{U}) \quad = \quad -\vec{\nabla}p - \rho g\hat{k}. \tag{2.1}$$

Here u, v and w are the velocity at x, y and z direction respectively; $\vec{U} = (u, v, w)$; p is the pressure of the fluid; ρ is the density of the fluid; g is the acceleration due to gravity; $\hat{k} = (0, 0, 1)$ is the unit vector in the vertical direction, and f is the Coriolis parameter associated with the Earth's rotation. The notation $\frac{D}{Dt}$ is the material derivative, representing the rate of change moving with a fluid particle. It is defined as,

$$\frac{D}{Dt} = \frac{\partial}{\partial t} + \vec{U} \cdot \vec{\nabla}. \tag{2.2}$$

2.1.1 f-plane Approximation

In the momentum equation (2.1), $\vec{\Omega} = (\Omega_x, \Omega_y, \Omega_z) = (0, \Omega\cos\theta, \Omega\sin\theta)$ is the angular velocity of the Earth in the local Cartesian system. The Earth rotates at $\Omega = 2\pi$ rad/day $= 0.73 \times 10^{-4}$ s^{-1} and θ is the latitude. f is defined to be $2\Omega\sin\theta$ and f is usually referred to as the Coriolis parameter or the Coriolis frequency. We can note that the full Coriolis term is of the following form,

$$2\vec{\Omega} \times \vec{U} = (-fv + 2\Omega w\cos\theta, fu, -2\Omega u\cos\theta). \tag{2.3}$$

However, the vertical component $-2\Omega u\cos\theta$ and the horizontal component $2\Omega w\cos\theta$ are usually negligible compared with the other terms in the vertical momentum equation. Hence, we generally approximate the Coriolis acceleration to be

$$2\vec{\Omega}\times\vec{U} = (-fv, fu, 0). \tag{2.4}$$

This is called the f-plane approximation. Under this approximation, the momentum equations can be written as,

$$\rho\big(\frac{Du}{Dt} - fv\big) = -p_x \tag{2.5}$$

$$\rho\big(\frac{Dv}{Dt} - fu\big) = -p_y \tag{2.6}$$

$$\rho\frac{Dw}{Dt} = -p_z - \rho g. \tag{2.7}$$

2.1.2 Boussinesq Approximation

For certain flows, Boussinesq 1903 suggested that the density change can be ignored except in the gravitational force term $\rho g\hat{k}$. A formal justification of the Boussinesq approximation is given in Spiegel and Veronis (1960) ([10])). This section will only present the basis of the approximation in an intuitive manner.
We can write density and pressure term as,

$$\rho = \rho_0 + \rho' \tag{2.8}$$

$$p = p_0 + p' \tag{2.9}$$

Here ρ_0 and p_0 are reference values, and they satisfy

$$\frac{dp_0}{dz} = -\rho_0 g. \tag{2.10}$$

ρ_0 is a constant; p_0 is a function of z only; ρ' is a very small value compared with the reference values ρ_0, i.e., $\rho' \ll \rho_0$.

Momentum Equation

Substituting (2.8), (2.9) and (2.10) into the momentum equation gives

$$(\rho_0 + \rho')(\frac{D\vec{U}}{Dt} + 2\vec{\Omega}\times\vec{U}) = -\vec{\nabla}p' - \rho' g\hat{k} \tag{2.11}$$

Dividing (2.11) by ρ_0, we have

$$(1+\frac{\rho'}{\rho_0})\big(\frac{D\vec{U}}{Dt}+2\vec{\Omega}\times\vec{U}\big)=-\frac{\vec{\nabla}p'}{\rho_0}-\frac{\rho'}{\rho_0}g\hat{k} \tag{2.12}$$

Since we assume $\rho' \ll \rho_0$, we can have that the term $\frac{\rho'}{\rho_0}$ is very small compared with 1 in the equation, while the contribution of the term $\frac{\rho'}{\rho_0}g\hat{k}$ cannot be neglected. Hence, the momentum equation after Boussinesq's approximation becomes

$$\frac{D\vec{U}}{Dt}+2\vec{\Omega}\times\vec{U}=-\frac{\vec{\nabla}p'}{\rho_0}-\frac{\rho'}{\rho_0}g\hat{k} \tag{2.13}$$

Continuity Equation

In the continuity equation

$$\frac{1}{\rho}\frac{D\rho}{Dt}+\vec{\nabla}\cdot\vec{U}=0, \tag{2.14}$$

For nearly incompressible flows the dominant balance in this equation is among u_x, v_y and w_z. Thus, the continuity equation is replaced by the incompressiblity condition

$$\vec{\nabla}\cdot\vec{U}=0. \tag{2.15}$$

However, this simplification does not apply in all situations. For example, for steady flows with large Mach numbers, large pressure changes can lead to large density changes. Or if the vertical scale of the flow is very large, the hydrostatic pressure variations can lead to large density changes as well.

Summary

The set of equations with Boussinesq approximation, after dropping the primes, is given by

$$\frac{D\vec{U}}{Dt}+2\vec{\Omega}\times\vec{U} = -\frac{\vec{\nabla}p}{\rho_0}-\frac{\rho}{\rho_0}g\hat{k} \tag{2.16}$$

$$\vec{\nabla}\cdot\vec{U} = 0 \tag{2.17}$$

$$\frac{D\rho}{Dt} = 0. \tag{2.18}$$

Here, the last density equation comes from internal energy equation and the derivation is omitted here.

2.2 Linearized Equations

When the fluid is at rest, we have that

$$\begin{aligned} \vec{U_b} &= (0,0,0) && (2.19)\\ \rho &= \rho_b(z) && (2.20)\\ p &= p_b(z). && (2.21) \end{aligned}$$

Since the fluid is not moving, the pressure and the density satisfy the hydrostatic condition

$$\frac{dp_b}{dz} = -\rho_b g \tag{2.22}$$

Now assume there is a small disturbance in the fluid

$$\begin{aligned} \vec{U} &= \vec{U_b} + \vec{U'} && (2.23)\\ p &= p_b + p' && (2.24)\\ \rho &= \rho_b + \rho'. && (2.25) \end{aligned}$$

Here, $\vec{U'}$, p' and ρ' are the small disturbances of the velocity field, the pressure and the density.
After substituting the expressions for $\vec{U}$, p and ρ into the fully nonlinear equations and further assuming the wave amplitude is small, all the nonlinear terms in the momentum equation and in the density equation will be neglected. The linearized equations, after dropping the primes, are

$$\begin{aligned} \frac{\partial \vec{U}}{\partial t} + 2\vec{\Omega} \times \vec{U} &= -\frac{1}{\rho_0}\vec{\nabla} p - \frac{\rho g}{\rho_0}\hat{k}, && (2.26)\\ \frac{\partial \rho}{\partial t} + w\frac{d\rho_b}{dz} &= 0, && (2.27)\\ \vec{\nabla} \cdot \vec{U} &= 0. && (2.28) \end{aligned}$$

The equations above can also be written as

$$\begin{aligned} \frac{\partial u}{\partial t} - fv &= -\frac{1}{\rho_0}\frac{\partial p}{\partial x}, && (2.29)\\ \frac{\partial v}{\partial t} + fu &= -\frac{1}{\rho_0}\frac{\partial p}{\partial y}, && (2.30)\\ \frac{\partial w}{\partial t} &= -\frac{1}{\rho_0}\frac{\partial p}{\partial z} - \frac{\rho g}{\rho_0}, && (2.31)\\ \frac{\partial \rho}{\partial t} + w\frac{d\rho_b}{dz} &= 0, && (2.32)\\ \frac{\partial u}{\partial x} + \frac{\partial v}{\partial y} + \frac{\partial w}{\partial z} &= 0. && (2.33) \end{aligned}$$

2.2.1 Buoyancy Frequency

We introduce the definition for the buoyancy frequency N here. It is defined by

$$N^2(z) = -\frac{g}{\rho_0}\frac{d\rho_b}{dz}. \tag{2.34}$$

Equation (2.32) can be written as

$$\frac{\partial \rho}{\partial t} - w\frac{N^2\rho_0}{g} = 0. \tag{2.35}$$

The importance of $N(z)$ in stratified flows will be discussed in the next section.

2.2.2 Constant N

Firstly, the linear stratification, i.e. constant N, is considered here, since we want to find analytic expression for the dispersion relation. Assume a plane wave solution

$$\begin{aligned} u &= u_0 e^{i(kx+ly+mz-\sigma t)}, && (2.36)\\ v &= v_0 e^{i(kx+ly+mz-\sigma t)}, && (2.37)\\ w &= w_0 e^{i(kx+ly+mz-\sigma t)}, && (2.38)\\ p &= p_0 e^{i(kx+ly+mz-\sigma t)}, && (2.39)\\ \rho &= \rho_0 e^{i(kx+ly+mz-\sigma t)}. && (2.40) \end{aligned}$$

Substituting these expressions into (2.29) to (2.33), we obtain the dispersion relation,

$$\sigma^2 = \frac{N^2k^2 + f^2m^2}{k^2 + m^2}, \tag{2.41}$$

where l has been set to be 0. The result indicates that if we do not include rotation, the frequency, the phase speed and the group velocity will be smaller. The first set of figures is of the frequency σ; the second set of figures is of the phase speed c and the third set of figures is of the group velocity c_g. All of them are plotted as functions of wavenumber k. For mode-one waves, using $f = 10^{-4}$ s^{-1}, $H = 3$ km and $N = 10^{-3}$ s^{-1}, hence

$$m = \frac{\pi}{H} = \frac{\pi}{3000}. \tag{2.42}$$

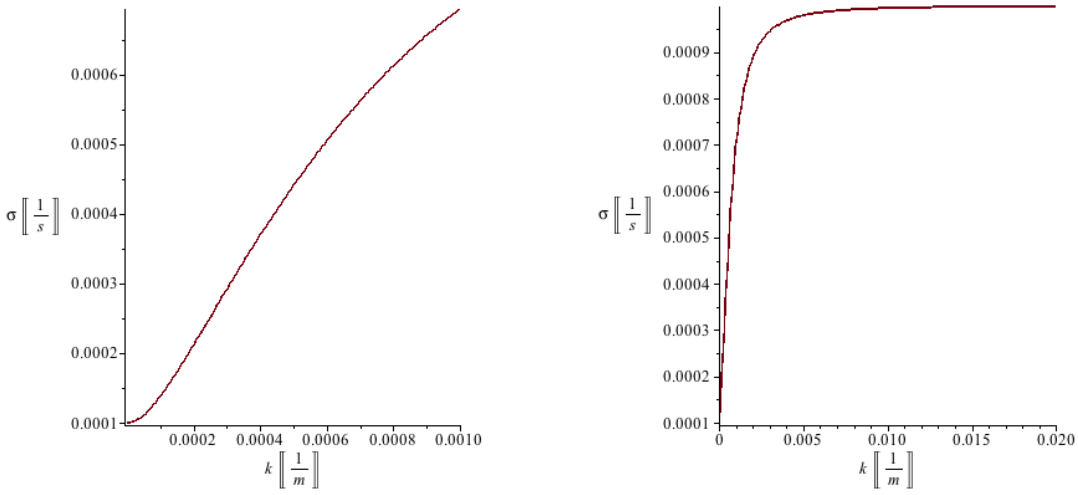

Figure 2.1: Frequency vs wavenumber for the linearized equations with rotation.

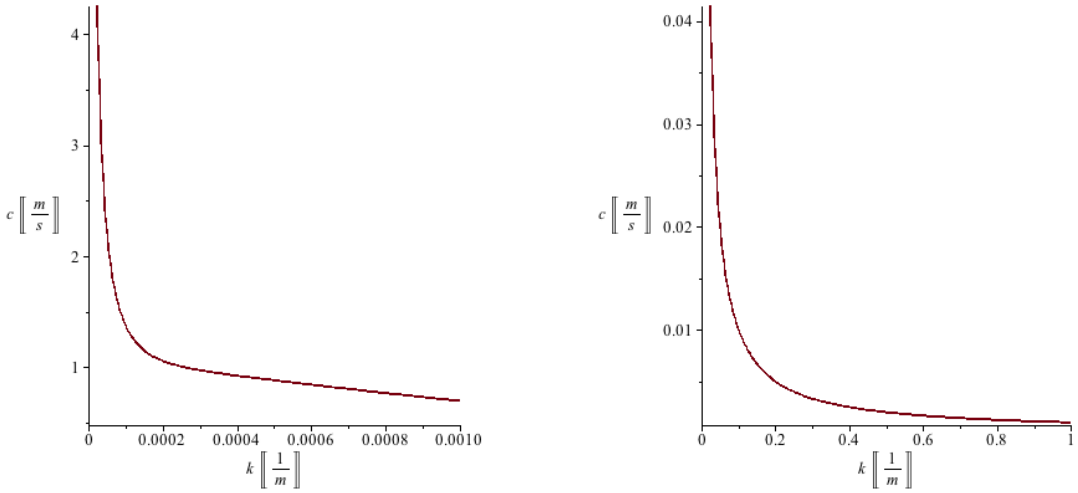

Figure 2.2: Phase speed vs wavenumber for the linearized equations with rotation.

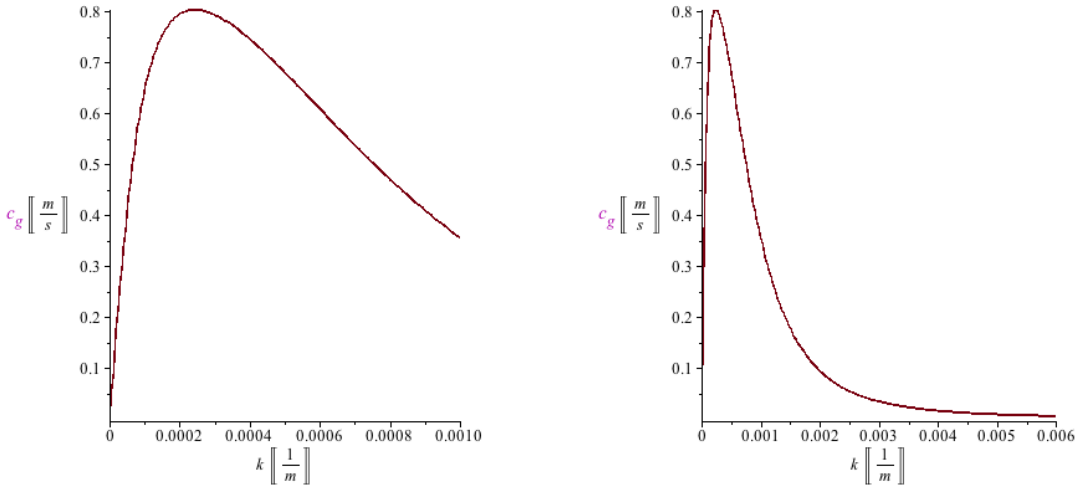

Figure 2.3: Group velocity vs wavenumber for the linearized equations with rotation.

From the dispersion relation,

$$\sigma \sim \begin{cases} f & \text{as k} \to 0 \\ N & \text{as k} \to \infty. \end{cases} \tag{2.43}$$

$$c = \frac{\sigma}{k} \sim \begin{cases} \frac{f}{k} & \text{as k} \to 0 \\ \frac{N}{k} & \text{as k} \to \infty. \end{cases} \tag{2.44}$$

$$c_g = \frac{\partial \sigma}{\partial k} \sim \begin{cases} \frac{(N^2-f^2)}{fm^2}k & \text{as k} \to 0 \\ \frac{m^2(N^2-f^2)}{N}\frac{1}{k^3} & \text{as k} \to \infty. \end{cases} \tag{2.45}$$

As the wave becomes infinitely long, $k \to 0$, the frequency of the wave goes to f, the phase speed c goes to infinity and the group velocity c_g goes to 0.

2.2.3 Non-constant N

Secondly, we consider the case when the stratification is not linear, i.e., $N = N(z)$. An equation for w can be obtained from eliminating all the other variables in (2.29) to (2.33).

$$\frac{\partial^2}{\partial t^2}\nabla^2 w + N^2 \nabla_H^2 w + f^2 \frac{\partial^2 w}{\partial z^2} = 0, \tag{2.46}$$

where $\nabla^2 = \frac{\partial^2}{\partial x^2} + \frac{\partial^2}{\partial y^2} + \frac{\partial^2}{\partial z^2}$ and $\nabla_H^2 = \frac{\partial^2}{\partial x^2} + \frac{\partial^2}{\partial y^2}$. Now we assume the solutions have the following form,

$$\begin{aligned} u &= u_0(z)e^{i(kx+ly-\sigma t)}, && (2.47)\\ v &= v_0(z)e^{i(kx+ly-\sigma t)}, && (2.48)\\ w &= \phi(z)e^{i(kx+ly-\sigma t)}, && (2.49)\\ p &= p_0(z)e^{i(kx+ly-\sigma t)}, && (2.50)\\ \rho &= \rho_0(z)e^{i(kx+ly-\sigma t)}. && (2.51) \end{aligned}$$

Substituion into the w-equation (2.46) gives

$$\frac{d^2\phi}{dz^2} + \frac{(N^2-\sigma^2)(k^2+l^2)}{\sigma^2-f^2}\phi = 0. \tag{2.52}$$

Defining

$$m^2(z) = \frac{(N^2-\sigma^2)(k^2+l^2)}{\sigma^2-f^2}, \tag{2.53}$$

(2.52) becomes

$$\frac{d^2\phi}{dz^2} + m^2\phi = 0. \tag{2.54}$$

Now we impose the rigid-lid approximation, which is used throughout this thesis. There is no solution satisfying (2.54) and the rigid-lid approximation when $m^2 < 0$ everywhere, thus we only consider the fluid layer where $m^2 > 0$. Following this argument, we have

$$f < \sigma < N. \tag{2.55}$$

Rayleigh gives the solution for the particular case when N is constant.

$$\phi = \sin\big(m(z+H)\big). \tag{2.56}$$

Here H is the water depth; $mH = n\pi$, where n is any positive integer. This solution can be viewed as linear combination of the solutions from the constant N case, since

$$\sin\big(m(z+H)\big) = \frac{1}{2}\big(e^{i(m(z+H))} - e^{-i(m(z+H))}\big). \tag{2.57}$$

Following the Rayleigh solution, we can get the dispersion relation,

$$\sigma_n^2 = \frac{(k^2+l^2)N^2H^2 + f^2n^2\pi^2}{n^2\pi^2 + (k^2+l^2)H^2}. \tag{2.58}$$

Here n represents the mode number. For example, when $n = 1$, the wave is called mode-1 wave. The phase speed and group velocity are given as,

$$\vec{c} = \frac{\sigma_n}{k^2 + l^2}(k, l), \tag{2.59}$$

$$\vec{c_g} = (\frac{\partial \sigma_n}{\partial k}, \frac{\partial \sigma_n}{\partial l}). \tag{2.60}$$

Further calculations can show $c_g \ll c$ when $f \neq 0$. The results also indicate that if we do not include rotation, the frequency σ will be smaller thus the phase speed c will be smaller, but the group velocity c_g will be larger.

2.3 Dubreil-Jacotin-Long (DJL) Equation

We now derive an exact solitary wave solution of the fully nonlinear equations (2.16) to (2.18). The DJL equation ([42]) describes two dimensional (x, z) waves of permanent form propagating with constant speed. Since the flow is incompressible, a stream function ψ can be defined with

$$u = \psi_z \tag{2.61}$$

$$w = -\psi_x. \tag{2.62}$$

The curl of the momentum equation under the Boussinesq approximation gives the vorticity equation

$$\frac{\partial}{\partial t}\nabla^2\psi + J(\nabla^2\psi, \psi) = g\frac{\rho_x}{\rho_0}. \tag{2.63}$$

Then re-write the density equation in terms of the Jacobian operator,

$$\frac{\partial \rho}{\partial t} + J(\rho, \psi) = 0 \tag{2.64}$$

with boundary conditions

$$\psi \to 0 \quad \text{as } x \to \pm\infty \tag{2.65}$$

$$\rho \to \bar{\rho}(z) \quad \text{as } x \to \pm\infty. \tag{2.66}$$

Here $\bar{\rho}(z)$ is the undisturbed density profile in the far field, and J is the Jacobian operator

$$J(A, B) = A_x B_z - A_z B_x. \tag{2.67}$$

We are interested in rightward propagating waves with constant phase speed c that maintain their shapes while they travel, i.e., solutions of the form

$$\psi(x,z,t) = \psi(x-ct,z) \tag{2.68}$$
$$\rho(x,z,t) = \rho(x-ct,z). \tag{2.69}$$

Using these, (2.63) and (2.64) become

$$J(\nabla^2\psi, \psi - cz) = g\frac{\rho_x}{\rho_0}, \tag{2.70}$$
$$J(\rho, \psi - cz) = 0. \tag{2.71}$$

Equation (2.71) indicates that ρ and $\psi - cz$ are functionally related, which can be written as

$$\rho = F(\psi - cz) \tag{2.72}$$

for some function F. Using the far field boundary condition when $x \to \pm\infty$

$$F(\psi - cz) \to F(-cz), \tag{2.73}$$
$$\rho \to \bar{\rho}(z), \tag{2.74}$$

hence

$$F(-cz) = \bar{\rho}(z) \quad \Rightarrow \quad F(z) = \bar{\rho}(-\frac{z}{c}). \tag{2.75}$$

Now we define a function $\zeta(x,z)$ as the vertical displacement of the streamline passing through the point (x,z). Then the density profile can be related to the far-field unperturbed density field via

$$\rho(x,z) = \bar{\rho}(z - \zeta(x,z)). \tag{2.76}$$

Combined with the function F, we have

$$\rho = F(\psi - cz) = \bar{\rho}(z - \frac{\psi}{c}) = \bar{\rho}(z - \zeta), \tag{2.77}$$

which implies that

$$\psi(x,z) = c\zeta(x,z). \tag{2.78}$$

Substitution of the equality (2.78) into the equation (2.70) and expanding ρ_x gives

$$J(c\nabla^2\zeta, c\zeta - cz) = g\frac{\rho_x}{\rho_0} = N^2(z-\zeta)\zeta_x, \tag{2.79}$$

where (2.76) has been used for the last step. Since $\zeta_x = J(\zeta, z) = J(\zeta, z-\zeta)$, we can further write the right hand side of (2.79) as

$$N^2(z-\zeta)J(\zeta, z-\zeta) \;\; = \;\; J(N^2(z-\zeta)\zeta, z-\zeta). \tag{2.80}$$

Then (2.79) can again be written as

$$J\big(\nabla^2\zeta + \frac{N^2(z-\zeta)}{c^2}\zeta, \zeta - z\big) = 0. \tag{2.81}$$

Hence, $\nabla^2\zeta + \frac{N^2(z-\zeta)}{c^2}\zeta$ and $\zeta - z$ are functionally related, i.e.,

$$\nabla^2\zeta + \frac{N^2(z-\zeta)}{c^2}\zeta = G(\zeta - z) \tag{2.82}$$

for some function G. Imposing the far field boundary condition

$$\zeta \to 0 \quad \text{as } x \to \pm\infty, \tag{2.83}$$

gives $G(z) = 0$. Thus,

$$\nabla^2\zeta + \frac{N^2(z-\zeta)}{c^2}\zeta = 0. \tag{2.84}$$

This is the Dubreil-Jacotin-Long (DJL) equation ([42]). From the derivation of the DJL equation, we can see that this equation is for waves with open streamlines. Open streamlines are streamlines that come from the far field and are not closed. However, this equation can be applied to closed streamlines as well, except that it is indeterminate.

Chapter 3

Weakly Nonlinear Equations

Fully nonlinear numerical models are usually time consuming and expensive to solve, although they can be very accurate and can be applied to waves of arbitrary amplitude. Weakly-nonlinear models can be a very efficient substitute. The focus of this section is on KdV-type equations, which have been widely used and which are appropriate under the small and long wave assumptions.

3.1 Derivation of the Ostrovsky Equation

The incompressibility condition and the fact that we are looking for solutions independent of y leads us to a scalar stream function formulation. Then we start with the governing equations (2.16) to (2.18) derived in Chapter 2, and follow a procedure similar to that used in the derivation of the vorticity equation in the section 2.3. The equations become

$$\frac{\partial}{\partial t}\nabla^2\psi + J(\nabla^2\psi, \psi) = g\frac{\rho_x}{\rho_0} + fv_z \tag{3.1}$$

$$v_t + f\psi_z = J(\psi, v) \tag{3.2}$$

$$\frac{\partial \rho}{\partial t} + J(\rho, \psi) = 0, \tag{3.3}$$

where $(u, w) = (\psi_z, -\psi_x)$. This set of equations is often referred to as a 2.5 dimension model since v can be non-zero. We assume that the unperturbed state is a state of rest with stratification $\rho = \bar{\rho}(z)$ so that

$$\rho = \bar{\rho}(z) + \rho'(x, z, t). \tag{3.4}$$

Defining

$$b = \frac{g\rho'}{\rho_0}, \tag{3.5}$$

the equations can be written as

$$\frac{\partial}{\partial t}\nabla^2\psi + J(\nabla^2\psi, \psi) = b_x + fv_z \tag{3.6}$$

$$v_t + f\psi_z = J(\psi, v) \tag{3.7}$$

$$\frac{\partial b}{\partial t} + N^2(z)\psi_x = J(\psi, b). \tag{3.8}$$

3.1.1 Boundary Conditions

To focus on internal waves we make the rigid lid approximation which eliminates surface waves, which also indicates there is no density perturbation on the top and bottom. We also assume that as $x \to \infty$, the water is undisturbed and at rest so that $u \to 0$. Thus, we have

$$\psi = b = 0 \quad \text{at } z = -H, 0 \tag{3.9}$$

$$\psi,\, b \to 0 \quad \text{as } x \to \infty. \tag{3.10}$$

3.1.2 Non-dimensionalization

The spatial coordinates and buoyancy frequency are scaled as

$$x = L\tilde{x} \tag{3.11}$$

$$u = U\tilde{u} \tag{3.12}$$

$$w = W\tilde{w} \tag{3.13}$$

$$z = H\tilde{z} \tag{3.14}$$

$$N(z) = N_0\tilde{N}(z), \tag{3.15}$$

where L is a typical wavelength, W is the vertical velocity scale, H is the water depth and N_0 is the typical value of $N(z)$. The vertical structure function, which will appear later in the derivation, is determined from the eigenvalue problem

$$\phi'' + \frac{N^2}{c_0^2}\phi = 0, \tag{3.16}$$

here the eigenvalue c_0 is the linear, long-wave speed and $\phi(z)$ gives the leading order vertical structure of the wave. Under the change of variables $z = H\tilde{z}$, (3.16) becomes

$$\phi'' + \frac{N^2H^2}{c_0^2}\phi = 0. \tag{3.17}$$

This indicates that $c_0 \sim NH$, thus we can choose the velocity and time scale to be

$$c = N_0 H \tag{3.18}$$

$$T = \frac{L}{c} = \frac{L}{N_0 H} \tag{3.19}$$

We assume that the amplitude perturbation is small compared to the unperturbed state, i.e., the horizontal velocity u of the wave is small compared with the linear propagation speed. By letting $U = \epsilon c$, we have

$$u = \epsilon c \tilde{u} = \epsilon N_0 H \tilde{u}. \tag{3.20}$$

Here ϵ is a small amplitude parameter. Now we set

$$\psi = \epsilon \Psi \tilde{\psi}, \tag{3.21}$$

Using $u = \psi_z$, we have

$$\psi_z = \epsilon N_0 H \tilde{u} = \frac{\epsilon \Psi}{H} \tilde{\psi}_{\tilde{z}}. \tag{3.22}$$

This gives us that

$$\Psi = \epsilon N_0 H^2. \tag{3.23}$$

From the incompressibility condition $u_x + w_z = 0$ we see that

$$W = \frac{H}{L} U = \epsilon \frac{N_0 H^2}{L}. \tag{3.24}$$

We also need to scale b so we set $b = B\tilde{b}$. Since we assume the perturbation is small, the two linear terms on the left hand side of equation (3.8) dominate. As a result, we need

$$b = \epsilon N_0^2 H \tilde{b}. \tag{3.25}$$

Now after substituting all these scaled variables and dropping the tildes, the governing equations (3.6) to (3.8) become

$$\frac{\partial}{\partial t}\psi_{zz} - b_x = \epsilon J(\psi, \psi_{zz}) - \mu \frac{\partial}{\partial t}\psi_{xx} + \epsilon\mu J(\psi, \psi_{xx}) + \delta v_z \tag{3.26}$$

$$v_t + \psi_z = \epsilon J(\psi, v) \tag{3.27}$$

$$\frac{\partial}{\partial t} b + N^2(z)\psi_x = \epsilon J(\psi, b), \tag{3.28}$$

where $\mu = \left(\frac{H}{L}\right)^2$, ϵ can be viewed as $\frac{a}{H}$, $\delta = \frac{f^2 L^2}{c^2}$ is the inverse square of the Rossby number and a is a typical wave amplitude. For all the scaling and the following derivations, we assume $H \ll L$ and $a \ll H$, i.e., $\epsilon \ll 1$, $\mu \ll 1$ and $\delta \ll 1$.

3.1.3 Asymptotic Expansion

Since we have three small parameters ϵ, μ and δ, we can expand ψ and b as an asymptotic series:

$$\begin{aligned}
\psi &\sim \psi^{(0)} + \epsilon\psi^{(1,0,0)} + \mu\psi^{(0,1,0)} + \delta\psi^{(0,0,1)} + h.o.t, && (3.29)\\
b &\sim b^{(0)} + \epsilon b^{(1,0,0)} + \mu b^{(0,1,0)} + \delta b^{(0,0,1)} + h.o.t, && (3.30)\\
v &\sim v^{(0)} + \epsilon v^{(1,0,0)} + \mu v^{(0,1,0)} + \delta v^{(0,0,1)} + h.o.t, && (3.31)
\end{aligned}$$

where *h.o.t.* stands for higher order terms. We assume $\psi^{(0)}$ is separable as we are interested in horizontally propagating waves, so that

$$\psi^{(0)} = \eta(x,t)\phi(z). \tag{3.32}$$

Since the wave will change its shape while propagating, we will find that

$$\eta_t \sim -c_0\eta_x - \epsilon R(x,t) - \mu Q(x,t) - \delta T(x,t) + \epsilon^2 S(x,t) + h.o.t.. \tag{3.33}$$

Here, and in the following, by asymptotic we mean as ϵ, μ and δ all go to 0, η satisfies (3.33). For the derivation below, we set x_0 to be the left boundary and t_0 to be the initial time.

$O(1)$ **problem:**

The leading-order equations are

$$\begin{aligned}
\frac{\partial}{\partial t}\psi^{(0)}_{zz} - b^{(0)}_x &= 0 && (3.34)\\
v^{(0)}_t + \psi^{(0)}_z &= 0 && (3.35)\\
\frac{\partial b^{(0)}}{\partial t} + N^2(z)\psi^{(0)}_x &= 0. && (3.36)
\end{aligned}$$

Using the leading-order part of (3.33), we have

$$\begin{aligned}
\phi'' + \frac{N^2(z)}{c_0^2}\phi &= 0 && (3.37)\\
v^{(0)}_t &= -\psi^{(0)}_z = -\eta(x,t)\phi'(z) && (3.38)\\
b^{(0)} &= \frac{\eta}{c_0}N^2(z)\phi(z) = -\frac{\eta}{c_0}\phi'', && (3.39)
\end{aligned}$$

where c_0 is a constant. Equation (3.37) is an eigenvalue problem for ϕ and c_0. The velocity in the y direction has the form

$$v^{(0)} = G(x,t)\phi'(z) \tag{3.40}$$

where, from (3.38),

$$G(x,t) = G(x,t_0) - \int_{t_0}^{t} \eta(x,t')dt'. \tag{3.41}$$

Here $G(x,t_0)$ is to be determined.

$O(\epsilon)$ problem:

The $O(\epsilon)$ equations are

$$-R\phi'' + \frac{\partial}{\partial t}\psi_{zz}^{(1,0,0)} - b_x^{(1,0,0)} = \eta\eta_x(\phi\phi''' - \phi'\phi'') \tag{3.42}$$

$$-\frac{N^2}{c_0}R\phi + \frac{\partial}{\partial t}b^{(1,0,0)} + N^2\phi_x^{(1,0,0)} = -c_0\eta\eta_x(\phi\phi''' - \phi'\phi''). \tag{3.43}$$

The v equation is not included here, since the two equations above do not involve v. We again look for separable solutions. The form of the nonlinear term on the right hand side suggests that we seek solutions of the form

$$\psi^{(1,0,0)} = \eta^2\phi^{(1,0,0)}(z) \tag{3.44}$$

$$b^{(1,0,0)} = \eta^2 D^{(1,0,0)}(z) \tag{3.45}$$

$$R = \alpha\eta\eta_x. \tag{3.46}$$

Thus the equation (3.42) becomes

$$\phi_{zz}^{(1,0,0)} + \frac{N^2}{c_0^2}\phi^{(1,0,0)} = -\frac{\alpha}{c_0}\phi'' - \frac{1}{c_0}(\phi\phi''' - \phi'\phi''). \tag{3.47}$$

If we multiply the left hand side of the equation by ϕ and integrate it from 0 to 1, the result equals 0 and this solvability condition is used to calculate the coefficients in this derivation. Hence, imposing the condition that the integral of the right hand side multiplied by ϕ should also equal to 0, we have the value for α,

$$\alpha = \frac{3}{2}\frac{\int_{-1}^{0}\phi'^3 dz}{\int_{-1}^{0}\phi'^2 dz}. \tag{3.48}$$

$O(\mu)$ problem:

Following a similar procedure for the $O(\mu)$ problem, we find that

$$Q = \beta\eta_{xxx}, \tag{3.49}$$

$$\beta = \frac{c_0}{2}\frac{\int_{-1}^{0}\phi^2 dz}{\int_{-1}^{0}\phi'^2 dz}. \tag{3.50}$$

Note that $\beta > 0$.

$O(\delta)$ **Problem**

Proceeding as in the previous cases, we have the following governing equations.

$$\frac{\partial}{\partial t}\psi_{zz}^{(0,0,1)} - b_x^{(0,0,1)} = v_z^{(0)} + T(x,t)\frac{N^2}{c^2}\phi \tag{3.51}$$

$$b_t^{(0,0,1)} + N^2\psi_x^{(0,0,1)} = -T(x,t)\frac{N^2}{c_0}\phi(z) \tag{3.52}$$

Here $T(x,t)$ comes from the equation (3.33). The equation for $v^{(0,0,1)}$ is not of interest here and we shall see later that it is not necessary to find $v^{(0,0,1)}$, so it is omitted. Again we assume the solutions are separable.

$$\psi^{(0,0,1)} = \eta^{(0,0,1)}(x,t)\phi^{(0,0,1)}(z), \tag{3.53}$$

$$b^{(0,0,1)} = \eta^{(0,0,1)}(x,t)D^{(0,0,1)}(z). \tag{3.54}$$

Then we use the expression for $v^{(0)}$, which is derived in the $O(1)$ problem. Equations (3.51) and (3.52) become,

$$\eta_t^{(0,0,1)}\phi_{zz}^{(0,0,1)} - \eta_x^{(0,0,1)}D^{(0,0,1)} = \big(T-G\big)\frac{N^2}{c^2}\phi, \tag{3.55}$$

$$\eta_t^{(0,0,1)}D^{(0,0,1)} + N^2\eta_x^{(0,0,1)}\phi^{(0,0,1)} = -T\frac{N^2}{c_0}\phi. \tag{3.56}$$

From here, we assume that $\eta_t^{(0,0,1)}$, $\eta_x^{(0,0,1)}$ and T are proportional to G. Thus, we set

$$T(x,t) = rG(x,t), \tag{3.57}$$

$$\eta_t^{(0,0,1)} = G(x,t). \tag{3.58}$$

In the latter equation we do not need a constant in front of $G(x,t)$, since we can always rescale $D^{(0,0,1)}(z)$ to make the constant to 1. Now we want to determine the value for r and that $\eta_x^{(0,0,1)}$ is proportional to G to the leading order. Integrating (3.58) we have

$$\eta^{(0,0,1)}(x,t) = \eta^{(0,0,1)}(x,t_0) + \int_{t_0}^{t} G(x,t')dt'. \tag{3.59}$$

Differentiating by x gives

$$\eta_x^{(0,0,1)}(x,t) = \eta_x^{(0,0,1)}(x,t_0) + \int_{t_0}^{t} G_x(x,t')dt'. \tag{3.60}$$

Recalling that

$$\eta_x = -\frac{1}{c_0}\eta_t + O(\epsilon,\mu,\delta), \tag{3.61}$$

and from the definition of G

$$G(x,t) = G(x,t_0) - \int_{t_0}^{t} \eta(x,t')dt', \tag{3.62}$$

we have

$$\begin{aligned} G_x(x,t) &= G_x(x,t_0) - \int_{t_0}^{t} \eta_x(x,t')dt' && (3.63)\\ &= G_x(x,t_0) - \int_{t_0}^{t} \big(-\frac{1}{c_0}\eta_t + O(\epsilon,\mu,\delta)\big)dt' && (3.64)\\ &= G_x(x,t_0) + \frac{1}{c_0}\eta(x,t) - \frac{1}{c_0}\eta(x,t_0) + O(\epsilon,\mu,\delta). && (3.65) \end{aligned}$$

Thus, using (3.62) gives us

$$\begin{aligned} \eta_x^{(0,0,1)}(x,t) &= \eta_x^{(0,0,1)}(x,t_0) + \int_{t_0}^{t} G_x(x,t')dt' && (3.66)\\ &= -\frac{1}{c_0}G(x,t) + \frac{1}{c_0}G(x,t_0) + \eta_x^{(0,0,1)}(x,t_0) && (3.67)\\ &\quad +(t-t_0)\big(G_x(x,t_0) - \frac{1}{c_0}\eta(x,t_0)\big) + O(\epsilon,\mu,\delta). && (3.68) \end{aligned}$$

We want $\eta_x^{(0,0,1)}(x,t)$ to be proportional to G to the leading order. Hence, in order to cancel the term growing linearly in time and the other terms in the equation (3.67), we now take the initial conditions for G to be

$$G_x(x,t_0) = \frac{1}{c_0}\eta(x,t_0) \tag{3.69}$$

and

$$\frac{1}{c_0}G(x,t_0) = \eta_x^{(0,0,1)}(x,t_0). \tag{3.70}$$

Here, we set

$$G(x_0,t_0) = 0, \tag{3.71}$$

and

$$G(x,t_0) = \frac{1}{c_0}\int_{x_0}^{x} \eta(x',t_0)dx'. \tag{3.72}$$

In this way, we have

$$\eta_x^{(0,0,1)}(x,t) = -\frac{1}{c_0}G(x,t) + O(\epsilon,\mu,\delta). \tag{3.73}$$

The initial condition for G specifies the initial value for $v^{(0)}$, i.e., the initial flow in the y direction. Now we substitute all the expressions into the governing equations, and we follow the procedures as for the previous cases. After eliminating $D^{(0,0,1)}$, the equations reduce to

$$\phi_{zz}^{(0,0,1)} + \frac{N^2}{c_0^2}\phi^{(0,0,1)} = (2r-1)\frac{N^2}{c_0^2}\phi(z). \tag{3.74}$$

By using the solvability condition, we have

$$r = \frac{1}{2}. \tag{3.75}$$

Until now, we have determined all the terms up to $O(\epsilon,\mu,\delta)$. The $O(\delta)$ term is $\delta T(x,t)$, where $T(x,t) = rG(x,t) = \frac{1}{2}\big(G(x,t_0) - \int_{t_0}^{t}\eta(x,t')dt'\big)$. Combined with the terms we found at $O(\epsilon)$ and $O(\mu)$, we have the equation for $\eta(x,t)$ as

$$\eta_t + c_0\eta_x + \epsilon\alpha\eta\eta_x + \mu\beta\eta_{xxx} = -\frac{\delta}{2}\int_0^t \eta dt' + \frac{\delta}{2c_0}\int_{x_0}^{x}\eta(x',0)dx'. \tag{3.76}$$

$O(\epsilon^2)$ Problem

The derivation at the $O(\epsilon^2)$ level is similar to that in the previous sub-sections. The details can be found at ([33]), and the equation obtained here is,

$$\big(\eta_t + c_0\eta_x + \epsilon\alpha\eta\eta_x + \mu\beta\eta_{xxx} + \epsilon^2\alpha_1\eta^2\eta_x\big)_t = -\frac{\delta}{2}\eta. \tag{3.77}$$

In this thesis, we call this the alternative Ostrovsky equation. The derivation of the alternative Ostrovsky equation was done by Lamb ([33]).

3.1.4 Properties of Alternative Ostrovsky equation

The integral form of the alternative Ostrovsky equation is

$$\eta_t + c_0\eta_x + \epsilon\alpha\eta\eta_x + \mu\beta\eta_{xxx} + \epsilon^2\alpha_1\eta^2\eta_x = -\frac{f^2}{2}\int_0^t \eta dt' + \frac{f^2}{2c_0}\int_{x_0}^{x}\eta(x',0)dx', \tag{3.78}$$

where t_0 is set to be 0. Since the wave profile decays as $x \to \infty$ for all t, we have the initial condition for η that

$$\int_{x_0}^{\infty} \eta(x', 0)dx' = 0. \tag{3.79}$$

If we consider the periodic solution on a domain $[0, L]$, the initial condition becomes

$$\int_{0}^{L} \eta(x', 0)dx' = 0. \tag{3.80}$$

This indicates that the initial condition for the alternative Ostrovsky equation has zero mass over the entire interval.
One thing we need to note here is that, a velocity v in the y direction has been speficied in the equation. To leading order,

$$v_{AO}^{(0)}(x, z, t) = \big(\frac{1}{c_0}\int_0^x \eta(x', 0)dx' - \int_{t_0}^t \eta(x, t')dt'\big)\phi'(z). \tag{3.81}$$

The Coriolis terms result in non-zero v and the diversion of energy from the leading wave to an inertia-gravity wave train trailing the leading solitary wave.

3.1.5 Ostrovsky Equation

If we use

$$\eta_t = -c_0\eta_x + O(\epsilon, \mu, \delta), \tag{3.82}$$

we can re-write the definition of G as

$$\begin{aligned} G(x,t) &= G(x,t_0) - \int_{t_0}^t \eta(x,t')dt' && (3.83)\\ &= G(x,t_0) + \frac{1}{c_0}\big(\int_{x_0}^x \eta(x',t)dx' - \int_{x_0}^x \eta(x',t_0)dx'\big) && (3.84)\\ &\quad - \int_{t_0}^t \eta(x_0,t')dt' + O(\epsilon,\mu,\delta). && (3.85)\end{aligned}$$

Here we substitute the expression for $G(x, t_0)$, which is determined in the previous section,

$$G(x, t_0) = \frac{1}{c_0}\int_{x_0}^x \eta(x', t_0)dx'. \tag{3.86}$$

Then we have

$$G(x,t) = \frac{1}{c_0}\int_{x_0}^{x} \eta(x',t)dx' - \int_{t_0}^{t} \eta(x_0,t')dt' + O(\epsilon,\mu,\delta). \tag{3.87}$$

We integrate (3.82) twice with respect to x on the domain $[x_0, x]$ and $[0, L]$, and once with respect to t on the domain $[t_0, t]$.

$$-\int_{o}^{L}\int_{x_0}^{x} \eta(x',t_0)dx'\,dx + \int_{o}^{L}\int_{x_0}^{x} \eta(x',t)dx'\,dx \tag{3.88}$$

$$= -c_0\int_{t_0}^{t}\int_{0}^{L} \eta(x',t')dx'\,dt' + c_0 L\int_{t_0}^{t} \eta(x_0,t')dt' + O(\epsilon,\mu,\delta). \tag{3.89}$$

Here we set

$$\int_{o}^{L}\int_{x_0}^{x} \eta(x',t_0)dx'\,dx \;=\; 0, \tag{3.90}$$

$$\int_{0}^{L} \eta(x',t)dx' = 0. \tag{3.91}$$

Hence, we can have

$$\int_{t_0}^{t} \eta(x_0,t')dt' = \frac{1}{c_0 L}\int_{o}^{L}\int_{x_0}^{x} \eta(x',t)dx'\,dx + O(\epsilon,\mu,\delta). \tag{3.92}$$

Substituting this expression into (3.87),

$$G(x,t) = \frac{1}{c_0}\int_{x_0}^{x} \eta(x',t)dx' - \frac{1}{c_0 L}\int_{o}^{L}\int_{x_0}^{x} \eta(x',t)dx'\,dx + O(\epsilon,\mu,\delta). \tag{3.93}$$

All the other steps are the same as the ones in the derivation of the alternative Ostrovsky equations, we can deduce the Ostrovsky equation

$$\left(\eta_t + c_0\eta_x + \epsilon\alpha\eta\eta_x + \mu\beta\eta_{xxx} + \epsilon^2\alpha_1\eta^2\eta_x\right)_x = \frac{\delta}{2c_0}\eta \tag{3.94}$$

Hence, the Ostrovsky equation and the alternative Ostrovsky equation are equivalent up to $O(\epsilon, \mu, \delta)$.

Properties of Ostrovsky Equation

For periodic wave solution on a domain $[0, L]$ and $x_0 = 0$, we integrate both sides of the Ostrovsky equation with respect to x to get

$$\eta_t + c_0\eta_x + \epsilon\alpha\eta\eta_x + \mu\beta\eta_{xxx} + \epsilon^2\alpha_1\eta^2\eta_x = \frac{f^2}{2c_0}\Big(\int_0^x \eta dx' - \frac{1}{L}\int_0^L\int_0^x \eta(x',t)dx'dx\Big) \tag{3.95}$$

The Ostrovsky equation has some integral quantities which are determined by the initial condition and are preserved in time. Three of the most important and commonly used quantities are the mass, energy and L^2 norm conservation laws ([45]) ([64]) ([47]), ([46]) ([20]).

$$I_1 = \int_0^L \eta(x,t)dx = 0 \tag{3.96}$$

$$I_2 = \int_0^L \big(\frac{\alpha}{6}\eta^3 + \frac{\alpha_1}{12}\eta^4 + \frac{\beta}{2}\eta_x^2 + \frac{f^2}{4c}(\partial_x^{-1}\eta)^2\big)dx = \text{const.} \tag{3.97}$$

$$I_3 = \int_0^L \eta^2(x,t)dx = \text{const.} \tag{3.98}$$

Here,

$$\partial_x^{-1}\eta = \int_0^L \eta dx - \frac{1}{L}\int_o^L \int_0^x \eta(x',t)dx'dx. \tag{3.99}$$

The derivations of these conservation laws are quite tedious, and not our interest in this thesis. Thus, they are omitted here.
A velocity v in the y direction has been speficied in the equation. To the leading order,

$$v_O^{(0)}(x,z,t) = \big(\frac{1}{c_0}\int_0^x \eta(x',t)dx' - \frac{1}{c_0 L}\int_0^L \int_0^x \eta(x',t)dx'\,dx\big)\phi'(z). \tag{3.100}$$

At the initial time, $v_{AO}^{(0)}(x,z,0) = v_O^{(0)}(x,z,0)$. As time increases, $v_{AO}^{(0)} = v_O^{(0)} + O(\epsilon,\mu,\delta)$. The initial velocity $v^{(0)}(x,z,0)$ is generally not 0. However, the initial velocity v in the fully nonlinear model is set to be 0. This provides another way to see the difference between the fully nonlinear model and the weakly nonlinear models.

3.2 KdV-type Equations

Both of the Ostrovsky and the alternative Ostrovsky equation are modifications of the KdV equation. They differ from the KdV equation only by the additional rotational terms, which result in the velocity in the y direction. If we set $f = 0$ and $\epsilon = \mu = 1$ in the Ostrovsky (or the alternative Ostrovsky equation), we have the eKdV equation or the Gardner equation.

$$\eta_t + c_0\eta_x + \alpha\eta\eta_x + \beta\eta_{xxx} + \alpha_1\eta^2\eta_x = 0 \tag{3.101}$$

If we remove the cubic term $\alpha_1\eta^2\eta_x$ in (3.101), i.e., up to $O(\epsilon,\mu)$ instead of $O(\epsilon^2)$, we have the KdV equation.

$$\eta_t + c_0\eta_x + \alpha\eta\eta_x + \beta\eta_{xxx} = 0. \tag{3.102}$$

3.2.1 Two-layer Fluid

For a two-layer fluid with the rigid-lid approximation, where the densities of each layer are comparable, Stanton and Ostrovsky in 1998 ([61]) have given the values for the coefficients of the eKdV equation (3.101),

$$c_0 = \sqrt{\frac{g' h_1 h_2}{h_1 + h_2}}, \tag{3.103}$$

$$g' = g\frac{\Delta\rho}{\rho_0}, \tag{3.104}$$

$$\alpha_1 = -\frac{3c_0}{8}\left(\frac{1}{h_1^2} + \frac{1}{h_2^2} + \frac{6}{h_1 h_2}\right), \tag{3.105}$$

$$\alpha = \frac{3c_0}{2}\left(\frac{1}{h_2} - \frac{1}{h_1}\right), \tag{3.106}$$

$$\beta = c_0\frac{h_1 h_2}{6}. \tag{3.107}$$

Here $\Delta\rho$ is the density difference of the two layers; ρ_0 is the reference density; g' is the reduced gravity; h_1 is the thickness of the top layer; h_2 is the thickness of the bottom layer. This two-layer approximation captures the wave behavior well when the nonlinear coefficient α approaches 0, i.e., the thermocline is close to the mid-depth $\frac{h_1+h_2}{2}$ and $h_1 \sim h_2$. ([23])

3.2.2 Solitary Wave Solutions

KdV equation

The nonlinear term $\alpha\eta\eta_x$ in the KdV equation (3.102) makes the properties of the waves very different than those of the linear waves. Nonlinear waves do not obey the superposition principle, thus it is usually very difficult to find analytic solutions. The last term in the equation, $\beta\eta_{xxx}$, is a dispersive term, which affects the wave frequency. As a result, waves of different wavelengths will propagate at different speeds. The linear long wave equation, $\eta_t + c_0\eta_x = 0$, is valid for wave amplitudes going to zero and wavelengths going to infinity. Hence, the nonlinear and dispersive terms in the KdV equation are corrections to account for weak nonlinearity and dispersion. In this way, the wave will not be infinitely small. There are many solutions to the KdV equation, among which solitary wave solutions have probably received the most attention. An intuitive way to view this is that, the competition between the nonlinear and dispersive terms have formed some certain balance. As a result, the wave has a stable configuration, which gives a solitary wave. The KdV

equation is completely integrable thus its solitary wave solutions are solitons. The solitary wave solution can be written as

$$\eta = \eta_0 \mathrm{sech}^2[\gamma(x - ct)] \tag{3.108}$$

where

$$c = c_0 + \frac{\eta_0 \alpha}{3} \tag{3.109}$$

$$\gamma^2 = \frac{\eta_0 \alpha}{12\beta}. \tag{3.110}$$

$\eta_0\alpha$ is positive since $\gamma^2 > 0$. The amplitudes of the wave solutions are not bounded, and the waves can be either elevations or depressions depending on the sign of α. The wavelength λ increases as the amplitude decreases.
For a continuously stratified fluid, which is the focus of this thesis, there are many internal wave modes. The linear phase speed c_0 is obtained by finding the eigenvalue of the Sturm-Louiville problem for the linear eigenmode. Among the different modal waves, mode-1 and mode-2 waves are the most common phenomena in the ocean.

eKdV/Gardner equation

Solitary wave solutions of the eKdV equation (3.101), most often called the Gardner equation, are solitons as well and can be written in many forms (Katutani & Yamasaki 1978 [56], Miles 1979[31], Ostrovsky & Stepanyants 1989[39]). One way to write the solution is

$$\eta = \frac{\eta_0}{b + (1 - b)\cosh^2\gamma(x - Vt)} \tag{3.111}$$

where

$$V = c_0 + \frac{\eta_0}{3}\left(\alpha + \frac{1}{2}\alpha_1\eta_0\right) \tag{3.112}$$

$$\gamma^2 = \frac{\eta_0(\alpha + \frac{1}{2}\alpha_1\eta_0)}{12\beta} \tag{3.113}$$

$$b = -\frac{\eta_0\alpha_1}{2\alpha + \alpha_1\eta_0}. \tag{3.114}$$

Wave solutions of the eKdV equation require $\eta_0\alpha_1(\eta_0 + \frac{2\alpha}{\alpha_1}) > 0$ since $\beta > 0$. If $\alpha_1 < 0$, we have one limit on the wave amplitude, i.e., $\eta_{lim1} = -\frac{2\alpha}{\alpha_1}$. The second limit of the wave amplitude is obtained by the finiteness of the solution, which gives $b < 1$ and $\eta_{lim2} = -\frac{\alpha}{\alpha_1}$. Many properties of the eKdV solutions depend on the signs of the nonlinear coefficients α_1 and α, which are enumerated below.

1. $\alpha_1 > 0 \quad \& \quad \alpha > 0$
   The waves can be either elevation or depression. There is a minimum amplitude for the waves of depression so that $\eta < -\frac{2\alpha}{\alpha_1}$, but there is no bound for waves of elevation.

2. $\alpha_1 > 0 \quad \& \quad \alpha < 0$
   The waves can be either elevation or depression. There is a minimum amplitude for the waves of elevation so that $\eta > -\frac{2\alpha}{\alpha_1}$, but there is no bound for waves of depression.

3. $\alpha_1 < 0 \quad \& \quad \alpha > 0$
   Only waves of elevation can exist. The limit for the wave amplitudes are that $\eta < -\frac{\alpha}{\alpha_1}$.

4. $\alpha_1 < 0 \quad \& \quad \alpha < 0$
   Only waves of depression can exist. The limit for the wave amplitudes are that $\eta > -\frac{\alpha}{\alpha_1}$.

Holloway *et al* (1997, 1999)[20, 19] have shown that the KdV type theories can manage to to model some wave evolution, which are not in the normal range of equations' validity. Stanton & Ostrovsky 1998 [61] have also found that the eKdV equation modeled the highly nonlinear waves they observed quite well.
Below are some schematic plots of the solitary wave solutions of the eKdV equation. The dashed lines in each of the plots show the limiting amplitudes of the waves.

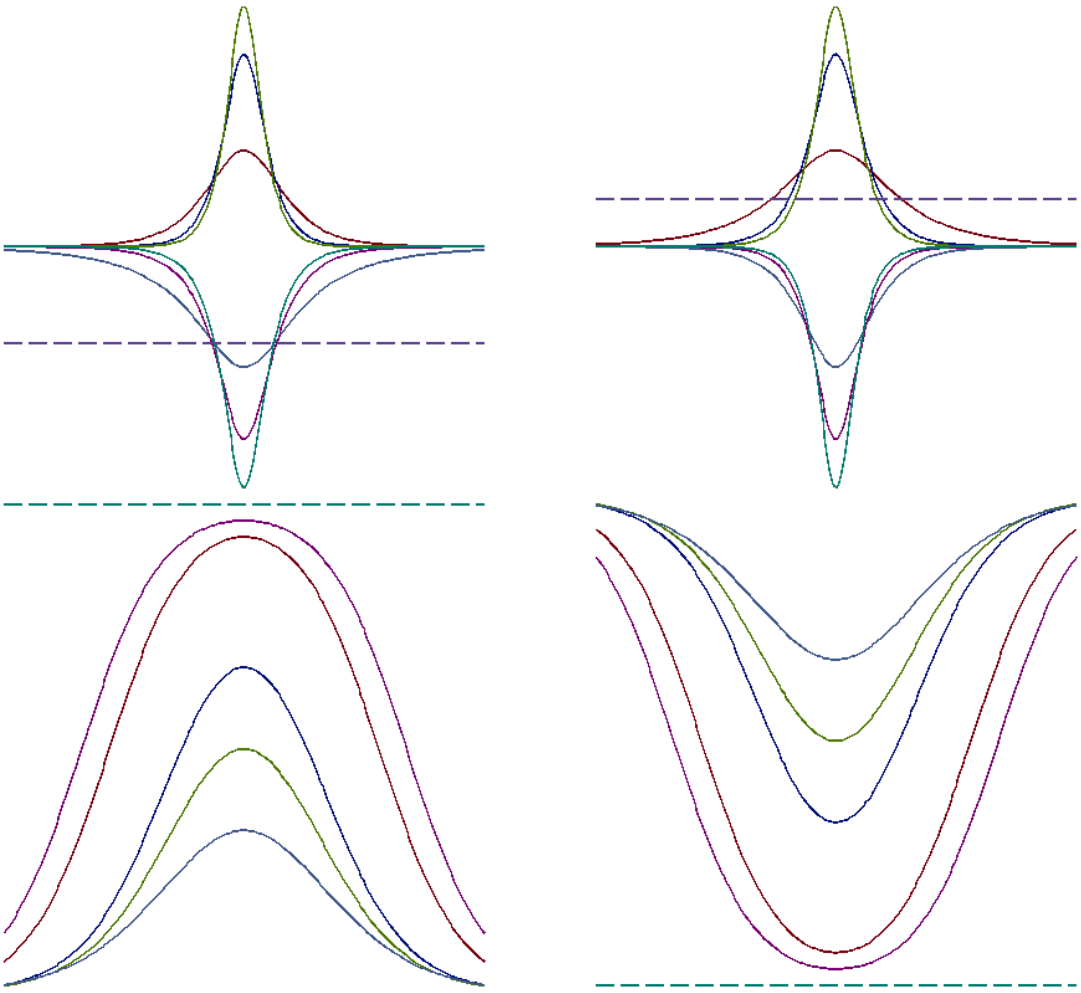

Figure 3.1: Possible solution plots, η VS x, of the eKdV equation are presented. The top left plot is for $\alpha > 0$, $\alpha_1 > 0$; the top right plot is for $\alpha < 0$, $\alpha_1 > 0$; the bottom left plot is for $\alpha > 0$, $\alpha_1 < 0$; the bottom right plot is for $\alpha < 0$, $\alpha_1 < 0$. When $\alpha_1 < 0$, the wave flattens out as its amplitude approaches the limit. The plots only show the qualitative behaviors of the solutions, thus the grids are not displayed on the plots.

3.3 Solution Analysis to KdV-type Equations

In this section, dispersion relations of different linearized KdV-type equations will be compared and graphs will be plotted for the corresponding frequency, phase speed and group velocity. I have used mode-one waves with $f = 10^{-4}$ s^{-1}, $H = 3$ km and $N = 10^{-3}$ s^{-1} to

plot all the graphs in this section, hence

$$m = \frac{\pi}{H} = \frac{\pi}{3000} \tag{3.115}$$

$$c_0 = \frac{N}{m} = \frac{3}{\pi} \tag{3.116}$$

$$\beta = \frac{N}{2m^3} = \frac{27}{2\pi} \times 10^6 \tag{3.117}$$

Here m is the vertical wavenumber. All of these coefficients are the same as those used in the section 2.2.

3.3.1 Linearized KdV Equation

$$\eta_t + c_0\eta_x + \beta\eta_{xxx} = 0 \tag{3.118}$$

Assume a plane wave solution

$$\eta = e^{i(kx-\sigma t)} \tag{3.119}$$

For equation (3.118), the dispersion relation is,

$$\sigma = c_0 k - \beta k^3 \tag{3.120}$$

From the dispersion relation, we can get the expression for the phase speed and group velocity.

$$c = \frac{\sigma}{k} = c_0 - \beta k^2 \tag{3.121}$$

$$c_g = \frac{\partial \sigma}{\partial k} = c_0 - 3\beta k^2 \tag{3.122}$$

Below are the graphs plotted for σ, phase speed c and group velocity c_g.

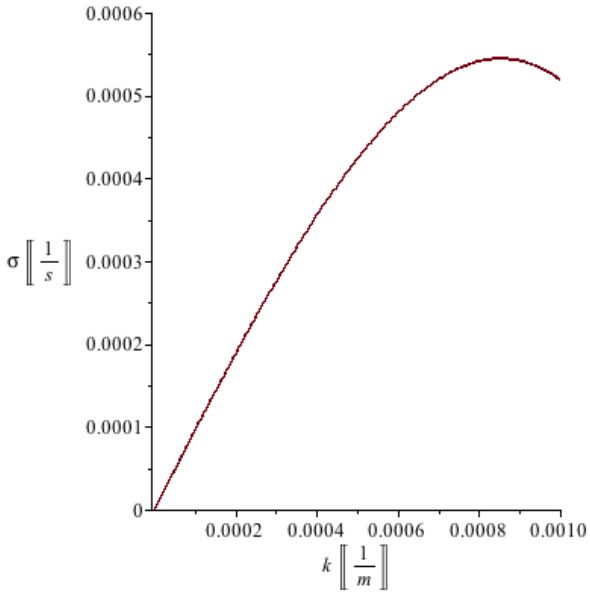

Figure 3.2: Frequency vs wavenumber for the linearized KdV equation.

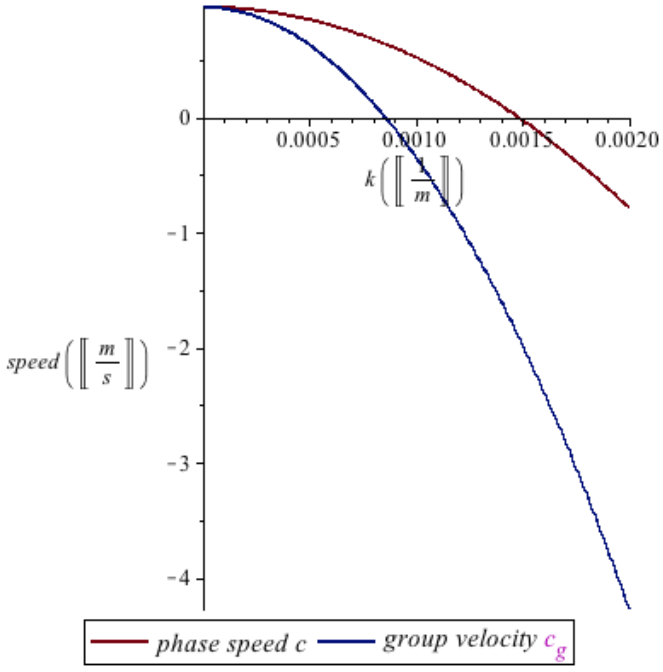

Figure 3.3: Phase speed vs wavenumber and group velcoity vs wavenumber for the linearized KdV equation.

Hence, we have,

$$\sigma \sim \begin{cases} c_0 k & \text{as k} \to 0 \\ -\beta k^3 & \text{as k} \to \infty. \end{cases} \tag{3.123}$$

$$c = \frac{\sigma}{k} \sim \begin{cases} c_0 & \text{as k} \to 0 \\ -\beta k^2 & \text{as k} \to \infty. \end{cases} \tag{3.124}$$

$$c_g = \frac{\partial \sigma}{\partial k} \sim \begin{cases} c_0 & \text{as k} \to 0 \\ -3\beta k^2 & \text{as k} \to \infty. \end{cases} \tag{3.125}$$

3.3.2 Linearized Ostrovsky Equation

$$(\eta_t + c_0 \eta_x + \beta \eta_{xxx})_x = \frac{f^2}{2c_0} \eta \tag{3.126}$$

Assume a plane wave solution

$$\eta = e^{i(kx - \sigma t)} \tag{3.127}$$

For equation (3.126), the dispersion relation is,

$$\sigma = c_0 k - \beta k^3 + \frac{1}{2c_o} \frac{f^2}{k} \tag{3.128}$$

From the dispersion relation, we can get the expression for the phase speed and group velocity,

$$c = \frac{\sigma}{k} = c_0 - \beta k^2 + \frac{1}{2c_o} \frac{f^2}{k^2}, \tag{3.129}$$

$$c_g = \frac{\partial \sigma}{\partial k} = c_0 - 3\beta k^2 - \frac{1}{2c_0} \frac{f^2}{k^2}. \tag{3.130}$$

Below are the graphs plotted for σ, phase speed c and group velocity c_g.

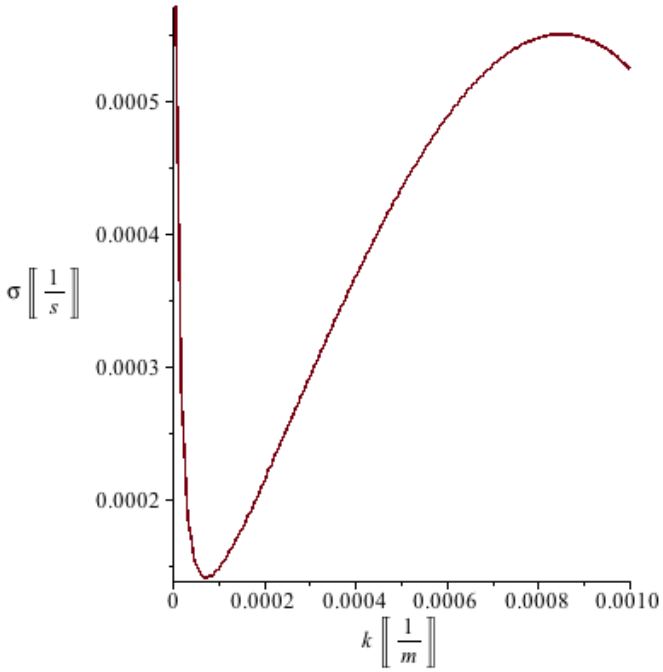

Figure 3.4: Frequency vs wavenumber for the linearized Ostrovsky equation.

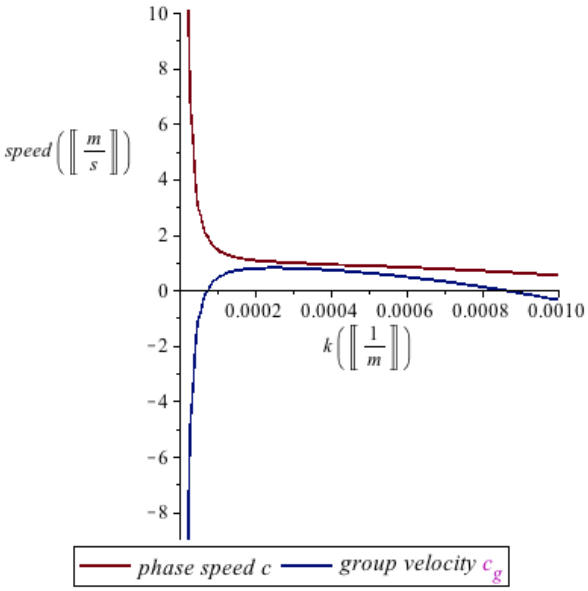

Figure 3.5: Phase speed vs wavenumber and group velocity vs wavenumber for the linearized Ostrovsky equation.

Hence, we have,

$$\sigma \sim \begin{cases} \frac{1}{2c_0}\frac{f^2}{k} & \text{as k} \to 0 \\ -\beta k^3 & \text{as k} \to \infty. \end{cases} \tag{3.131}$$

$$c = \frac{\sigma}{k} \sim \begin{cases} \frac{1}{2c_0}\frac{f^2}{k^2} & \text{as k} \to 0 \\ -\beta k^2 & \text{as k} \to \infty. \end{cases} \tag{3.132}$$

$$c_g = \frac{\partial \sigma}{\partial k} \sim \begin{cases} -\frac{1}{2c_0}\frac{f^2}{k^2} & \text{as k} \to 0 \\ -3\beta k^2 & \text{as k} \to \infty. \end{cases} \tag{3.133}$$

3.3.3 Linearized Alternative form of Ostrovsky Equation

$$(\eta_t + c_0\eta_x + \beta\eta_{xxx})_t = -\frac{f^2}{2}\eta \tag{3.134}$$

Assume a plane wave solution

$$\eta = e^{i(kx-\sigma t)} \tag{3.135}$$

For equation (3.134), the dispersion relation is,

$$\sigma^2 - (c_0 k - \beta k^3)\sigma - \frac{f^2}{2} = 0 \tag{3.136}$$

This is a quadratic equation, so we have two values for the frequencies.

$$\sigma_1 = \frac{(c_0 k - \beta k^3) + \sqrt{(c_0 k - \beta k^3)^2 + 2f^2}}{2} \tag{3.137}$$

$$\sigma_2 = \frac{(c_0 k - \beta k^3) - \sqrt{(c_0 k - \beta k^3)^2 + 2f^2}}{2} \tag{3.138}$$

Below are the graphs plotted for σ_1 and σ_2, the corresponding phase speeds and group velocities.

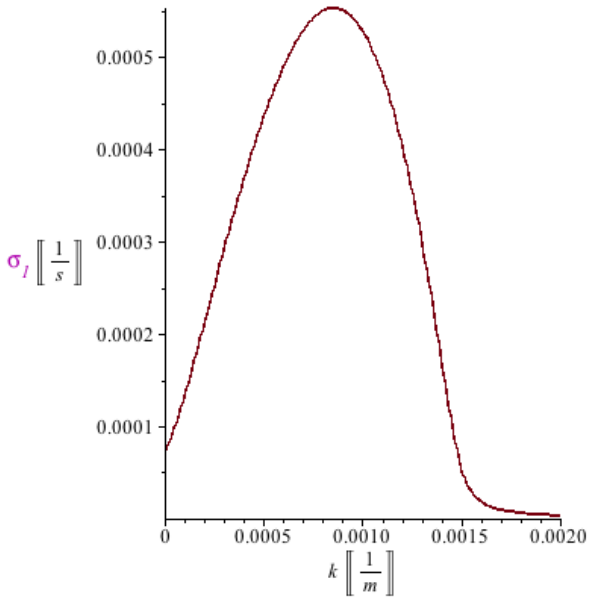

Figure 3.6: Frequency σ_1 vs wavenumber for the linearized alternative form of Ostrovsky equation.

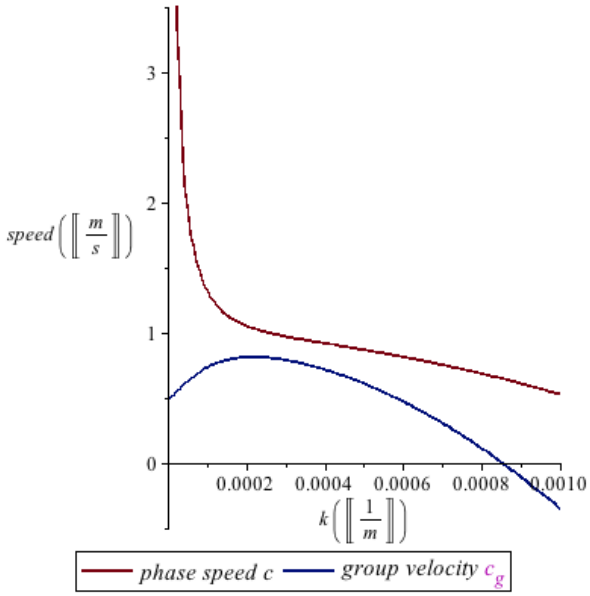

Figure 3.7: Phase speed c_1 vs wavenumber and group velocity c_{g1} vs wavenumber for the linearized alternative form of Ostrovsky equation.

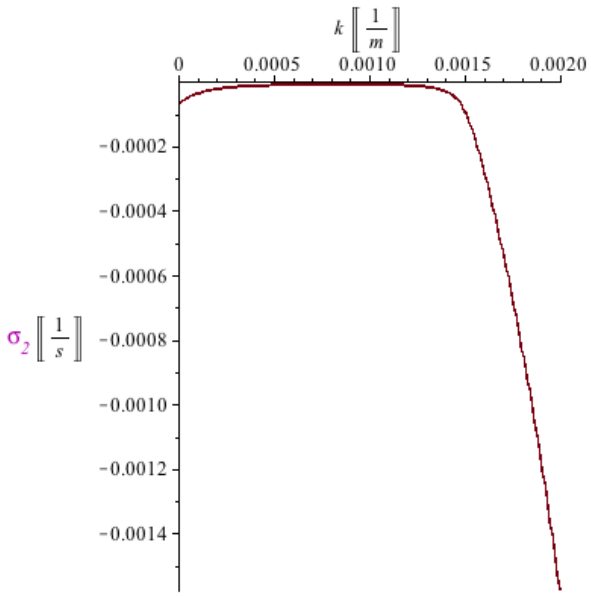

Figure 3.8: Frequency σ_2 vs wavenumber for the linearized alternative form of Ostrovsky equation.

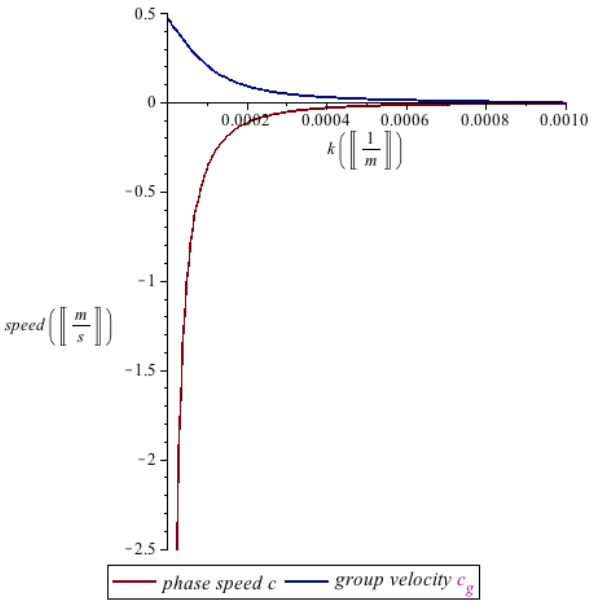

Figure 3.9: Phase speed c_2 vs wavenumber and group velocity c_{g2} vs wavenumber for the linearized alternative form of Ostrovsky equation.

Hence, we have,

$$\sigma_1 \sim \begin{cases} \frac{f}{\sqrt{2}} & \text{as k} \to 0 \\ \frac{f^2}{2\beta k^3} & \text{as k} \to \infty. \end{cases} \tag{3.139}$$

$$c_1 = \frac{\sigma}{k} \sim \begin{cases} \frac{f}{\sqrt{2}k} & \text{as k} \to 0 \\ \frac{f^2}{2\beta k^4} & \text{as k} \to \infty. \end{cases} \tag{3.140}$$

$$c_{g1} = \frac{\partial \sigma}{\partial k} \sim \begin{cases} c_0(\frac{1}{2} + \frac{1}{2\sqrt{2}f}) & \text{as k} \to 0 \\ -\frac{3}{2}\frac{f^2}{\beta k^4} & \text{as k} \to \infty. \end{cases} \tag{3.141}$$

$$\sigma_2 \sim \begin{cases} -\frac{f}{\sqrt{2}} & \text{as k} \to 0 \\ -\beta k^3 & \text{as k} \to \infty. \end{cases} \tag{3.142}$$

$$c_2 = \frac{\sigma}{k} \sim \begin{cases} -\frac{f}{\sqrt{2}k} & \text{as k} \to 0 \\ -\beta k^2 & \text{as k} \to \infty. \end{cases} \tag{3.143}$$

$$c_{g2} = \frac{\partial \sigma}{\partial k} \sim \begin{cases} \frac{1}{2}c_0 & \text{as k} \to 0 \\ -3\beta k^2 & \text{as k} \to \infty. \end{cases} \tag{3.144}$$

3.3.4 Comparisons

The graphs of the four frequencies, group velocities and phase speeds are shown below, where the plots of the fully linear equations (2.29) to (2.33), the linearized KdV equation (3.118), the linearized Ostrovsky equation (3.126) and the linearized alternative Ostrovsky equation (3.134) are represented by the red, yellow, black and the blue lines, respectively. Since we are only interested in the rightward propagating wave, the negative frequency in the linearized alternative Ostrovsky equation is not considered here.

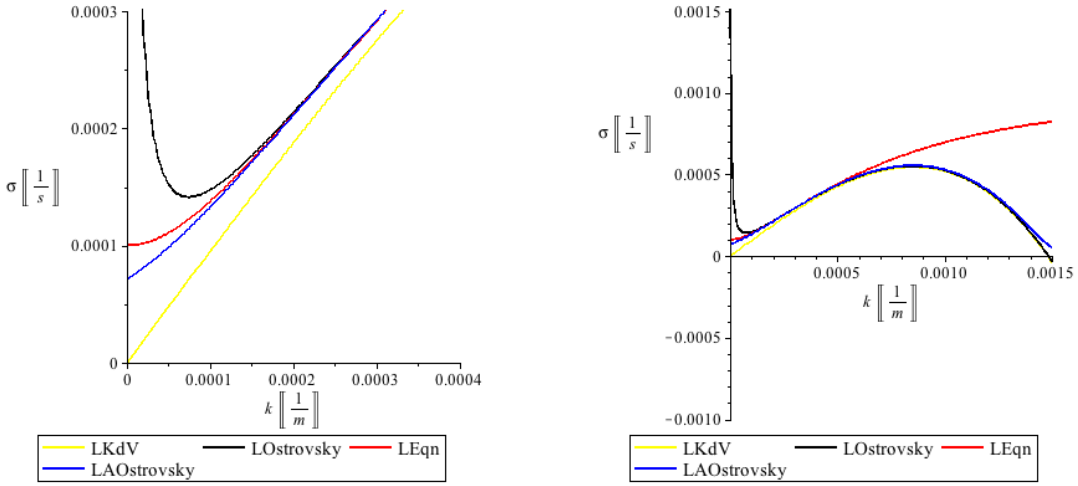

Figure 3.10: Frequency vs wavenumber.

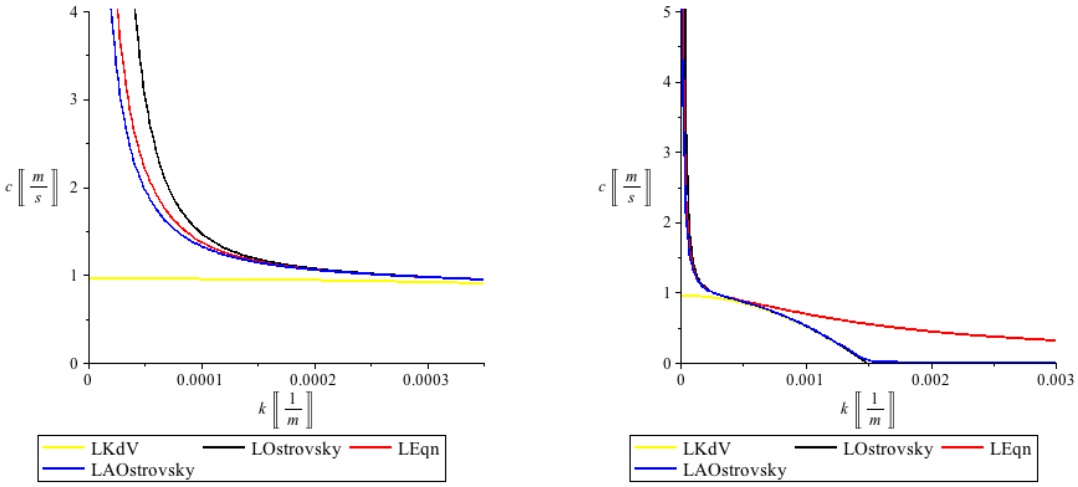

Figure 3.11: Phase speed vs wavenumber.

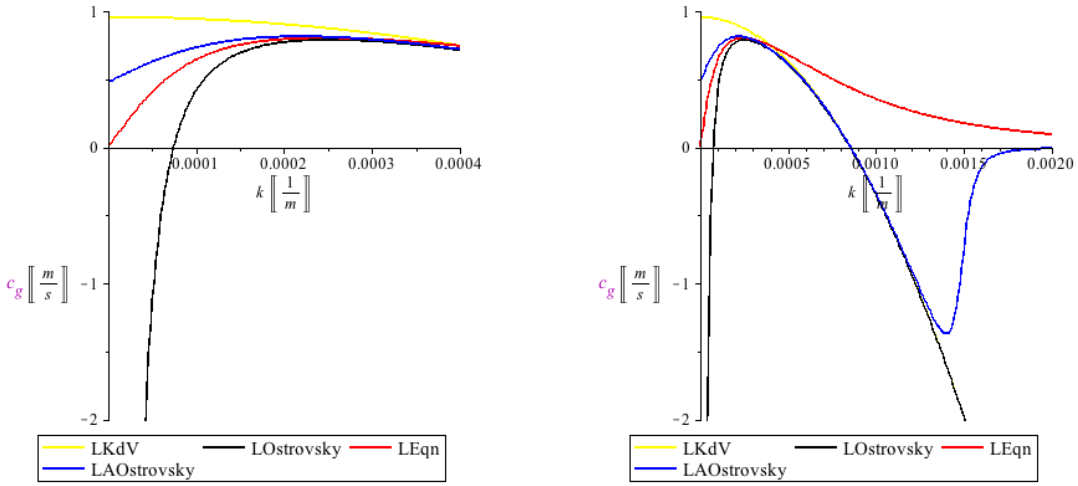

Figure 3.12: Group velocity vs wavenumber.

When k goes to 0, the frequencies for the fully linear equations (2.29) to (2.33) and for the linearized alternative Ostrovsky (3.134) go to constant values f and $\frac{f}{\sqrt{2}}$ separately, while both of the phase speeds are inversely proportional to k. Compared with the other three equations, the linearized KdV equation does not capture the behavior of the frequency and the phase speed very well, because of the absence of the Coriolis term in the equation. The linearized Ostrovsky equation fails to describe the behavior of the group velocity by giving it negative values when k approaches 0. Hence, compared with the result from the linearized momentum equations (2.29) to (2.33), the linearized alternative Ostrovsky equation seems to be the best of all the weakly nonlinear models.
However, when k is very small, i.e. $k < 0.0001\ m^{-1}$ in these plots, the weakly nonlinear equations do not perform very well. This is probably because that, rotational effect dominates when the wavelength becomes very long. Meanwhile, all of the weakly nonlinear models assume the rotation to be $O(\epsilon)$ in its derivation, which is not appropriate for very long waves. As a result, there is an intermediate valid range for the weakly nonlinear equations, i.e., around $0.0001\ m^{-1} < k < 0.0007\ m^{-1}$ in this case.
When k goes to ∞, none of the weakly-nonlinear equations (3.118), (3.126), (3.134) predict σ, c and c_g very well, since these equations are only valid for long waves.
We would expect the weakly nonlinear equations to be valid when the wave is suffiently long, which means the wavelength is much larger than the water depth. However, the wavelength cannot be too long, since the rotational effects are assumed to be small.

In this chapter, a new equation called the alternative Ostrovsky equation is presented as well as a short derivation of the Ostrovsky equation. Soliton solutions to the KdV and the Gardner equation are given. The frequencies, phase speeds and group velocities of

all the linearized equations are discussed. From the analysis of the linearized equations, the weakly nonlinear models are expected to perform well only within a certain range of wavenumber k.

Chapter 4

Numerical Model Setup

4.1 Fully Nonlinear Model: IGW

The equations used here are the incompressible Euler equations on an f-plane

$$\frac{D\vec{U}}{Dt} + 2\vec{\Omega} \times \vec{U} = -\frac{\vec{\nabla} p}{\rho_0} - \frac{\rho}{\rho_0} g\hat{k}, \tag{4.1}$$

$$\vec{\nabla} \cdot \vec{U} = 0, \tag{4.2}$$

$$\frac{D\rho}{Dt} = 0, \tag{4.3}$$

which are derived in Chapter 2. Here $2\vec{\Omega} \times \vec{U} = (-fv, fu, 0)$, i.e., f-plane. Rigid lid approximation is imposed on the water surface. The model was introduced by Lamb in 1994 ([34]) and ([35]), but the method is due to Bell, Collela and Glaz and Bell and Marcus.

4.1.1 Solitary Wave Initialization

The initial condition is a single solitary wave solution of the DJL equation derived in section 2.3:

$$\nabla^2 \zeta + \frac{N^2(z-\zeta)}{c^2}\zeta = 0. \tag{4.4}$$

The boundary conditions are

$$\zeta = 0 \quad \text{at} \quad z = 0, H \tag{4.5}$$

$$\zeta = 0 \quad \text{as} \quad x = \pm L, \tag{4.6}$$

where L is large. There are different techniques to solve the DJL equation. The IGW code uses a variational technique to minimize the kinetic energy for the functional ([5])

$$F(\zeta) = \frac{1}{H} \iint_R \int_0^{\zeta(x,z)} \big(\bar{\rho}(z - \zeta(x,z)) - \bar{\rho}(z-s)\big) ds\, dx\, dz, \tag{4.7}$$

where R is the computational subdomain in which the initial wave is computed. The available potential energy of the wave in an infinitely long domain is equal to $gHF(\zeta)$, which determines the amplitude of the solitary wave. Only mode-one solitary waves can be computed since the derivation of the DJL equation assumes a wave of permanent form and higher-mode solitary-like waves are generally accompanied by lower-mode, dispersive waves which creates energy loss from the leading wave and hence it is not steady ([62]). More details of solving the DJL equation can be found in ([35]).

4.1.2 Stratification, Topography and Boundary Conditions

The stratification considered in this model is

$$\rho(z) = \rho_1 + s_1 z + s_2 F(z, -Z_{pyc1}, d_{pyc1}) + s_3 F(z, -Z_{pyc2}, d_{pyc2}) \tag{4.8}$$

Here ρ_1 is the density at the surface; ρ_1, s_1, s_2 and s_3 are constants; F is a function that goes from a line with slope 0 to a line with slope 2. The transition occurs at Z_{pyc1} and Z_{pyc2}. d_{pyc1} and d_{pyc2} determine the thickness of the transition region. There is only one pycnocline in this stratification. $F(x, Z, d)$ is defined as,

$$F(x, Z, d) = (x - Z) + d(\log(\cosh(\frac{x - Z}{d})) + \log 2). \tag{4.9}$$

To have a clearer understanding of the stratification profile, we can re-write $F(x, Z, d)$ as

$$F(x, Z, d) = \int_Z^x \big(1 + \tanh(\frac{x' - Z}{d})\big) dx'. \tag{4.10}$$

We want the change of the density, i.e. F', to be constant at first, then slowly increases with depth, and remain constant at some value. $1 + \tanh(\frac{x'-Z}{d})$ is chosen to be F'. $\tanh(\frac{x'-Z}{d})$ allows us to pick the changing point and the thickness of this changing region. In addition, we can integrate it analytically.
The water depth is 500 m deep and the bottom is flat. The stratification is plotted in (4.1).

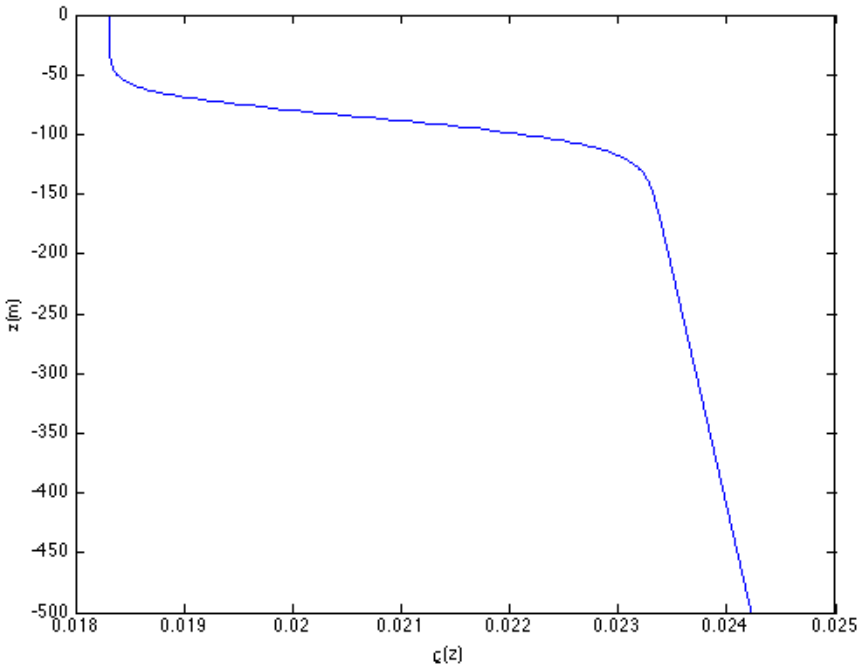

Figure 4.1: water depth vs density

The model uses the inflow and outflow boundary conditions. The flow is assumed to be hydrostatic at the right boundary. Waves pass through with little reflection however short hydrostatic waves will reflect off the boundary. In practice the right boundary is placed far enough from the region of interest that reflected waves are not a problem. u_t is specified at the left boundary.

4.1.3 Numerical Method

Projection Method

A second-order projection method is used to solve the model equations. The Helmholtz decomposition says that any vector $\vec{V}$ can be decomposed into the sum of a divergence free vector and the multiple of a strictly positive scalar function $a(x, z)$ and a gradient, i.e.,

$$\vec{V} = \vec{V}^D + a\vec{\nabla}\phi, \tag{4.11}$$

where $a(x,z)$ is a known given function. Then we can define a projection operator P_a that maps the vector $\vec{V}$ onto its divergence free part.

$$P_a(\vec{V}) = \vec{V}^D \tag{4.12}$$

P_a depends on both of the function a and the boundary conditions. Now we consider the momentum equation, which can be written as

$$\vec{U}_t + \frac{\vec{\nabla} p}{\rho_0} = -\vec{U}\cdot\vec{\nabla}\vec{U} - 2\vec{\Omega}\times\vec{U} - \frac{\rho}{\rho_0}g\hat{k}. \tag{4.13}$$

The left hand side of the equation has a divergence free vector $\vec{U}_t$ and a positive scalar times the gradient of the pressure term. Since the Boussinesq approximation has been made so $a(x,z)=1$ and $\vec{\nabla}\phi = \frac{\vec{\nabla}p}{\rho_0}$. Thus we can define a projection operator P_ρ so that

$$\vec{U}_t = P_\rho\big(-\vec{U}\cdot\vec{\nabla}\vec{U} - 2\vec{\Omega}\times\vec{U} - \frac{\rho}{\rho_0}g\hat{k}\big). \tag{4.14}$$

Computational Grids

Terrain-following (σ) coordinates are used. The grid cells are created by mapping the physical domain, with coordinates (x,z), to the computational domain, with coordinates (ξ,ζ), via the transformation

$$(\xi,\zeta) = (\xi(x,z),\zeta(x,z)). \tag{4.15}$$

Thus, the computational grid is a quadrilateral grid with I cells in the horizontal and J cells in the vertical. All the grid cells are unit squares and the grid points are evenly spaced. As a result, the equations calculated in the code are treated as functions of ξ and ζ.

4.2 Weakly Nonlinear Model

4.2.1 Alternative Ostrovsky equation solver

The model considered here is the integral form of the alternative Ostrovsky equation derived in Chapter 3. $[a,b]$ is the domain.

$$\eta_t + c_0\eta_x + \epsilon\alpha\eta\eta_x + \mu\beta\eta_{xxx} + \epsilon^2\alpha_1\eta^2\eta_x = -\frac{f^2}{2}\int_0^t \eta dt' + \frac{f^2}{2c_0}\int_a^x \eta(x',0)dx' \tag{4.16}$$

Solitary Wave Initialization

Based on our discussion on section (3.1.4), the initial condition of the wave profile shall satisfy

$$\int_a^b \eta(x', 0)dx' = 0. \tag{4.17}$$

Two different initial condition have been tested in order to fulfill the conservative integral. One initial condition is a combination of two internal waves with one solitary wave of depression and the other wave of elevation that is the same shape as the solitary wave. Each solitary wave is the solution of the eKdV equation.

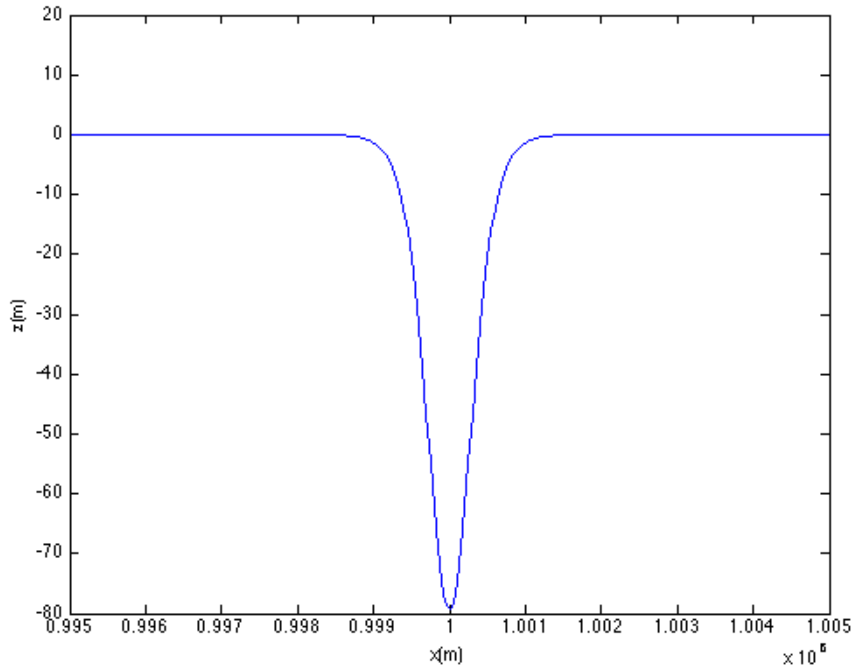

Figure 4.2: Solitary wave of depression. This is the wave solution of the eKdV equation.

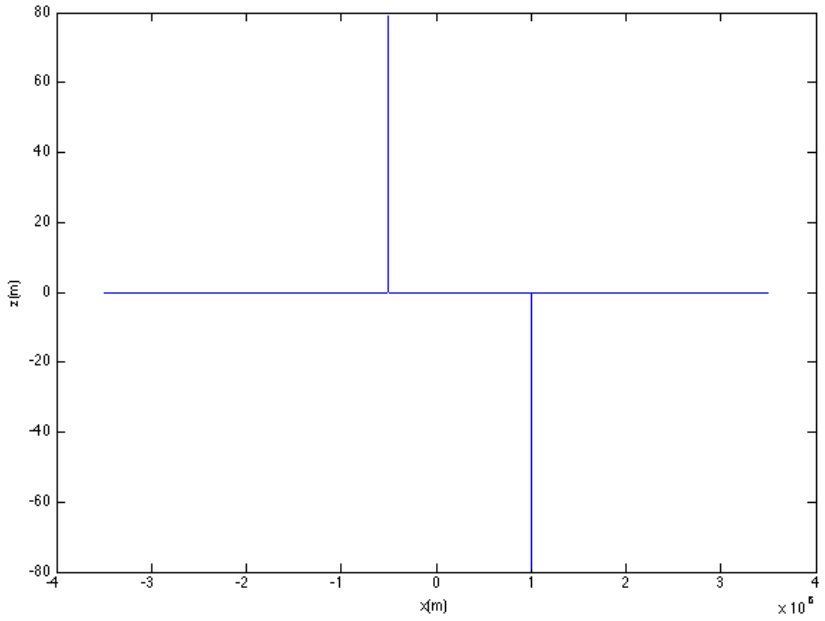

Figure 4.3: Wave initialization for the alternative Ostrovsky equation. The spikes show the locations of the initial wave of elevation and depression.

However, this initial condition has caused some oscillations at the tail of the leading depression solitary wave. All the plots below show that, η is constant but oscillates between about -3 m and +3 m behind the leading wave (to left of about -2e5 m). This oscillation is probably caused by the term $\frac{f^2}{2c_0}\int_a^x \eta(x',0)dx'$ on the right hand side of the alternative Ostrovsky equation. This term is independent of time and if the wave of elevation is too narrow and far away from the leading wave, obvious oscillation may be observed in the wave tail.

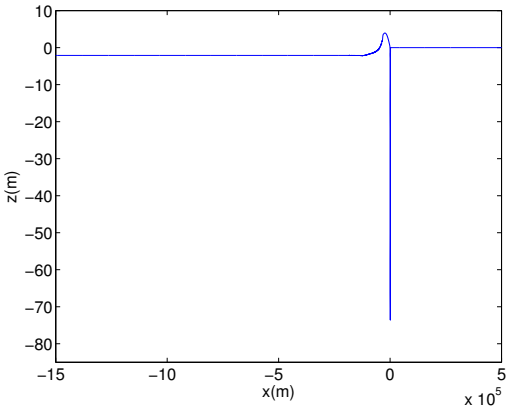

Figure 4.4: Time = 6000 s

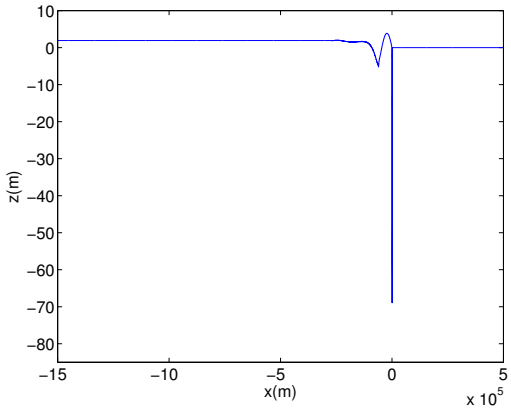

Figure 4.5: Time = 12000 s

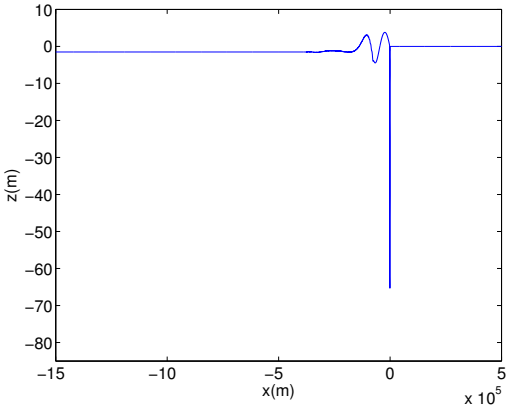

Figure 4.6: Time = 168000 s

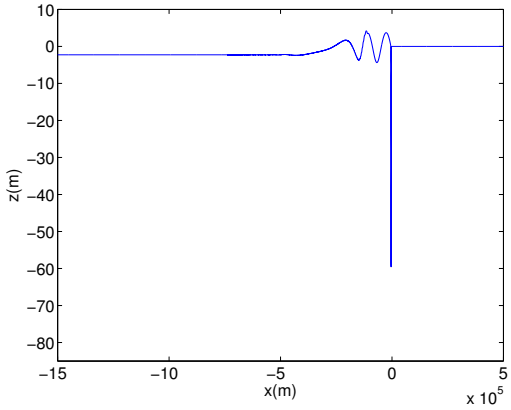

Figure 4.7: Time = 240000 s

This implies that instead of a second narrow wave of elevation far behind the leading wave, I should use a small long wave immediately behind the leading wave. Thus, the second initial condition is a combination of one depression solitary wave and a long elevation wave behind it.

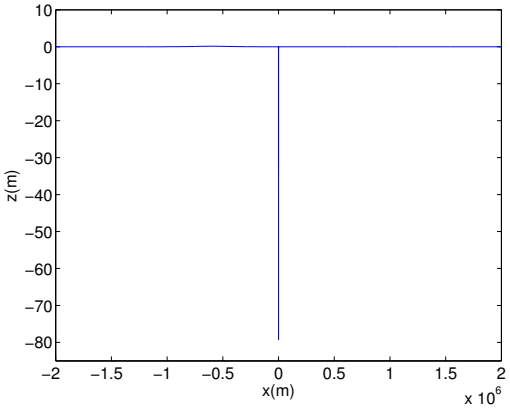

Figure 4.8: Initial wave profile

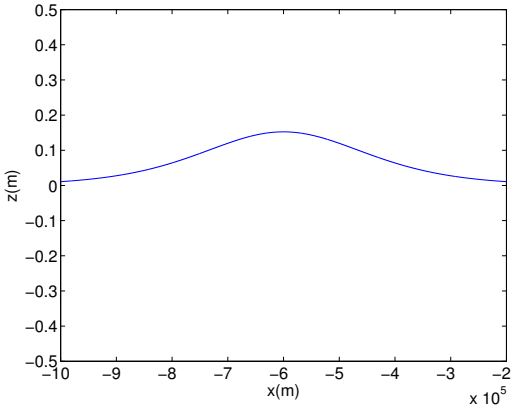

Figure 4.9: Zoomed in view of the initial elevation

Here the wavelength of the elevation wave is around 1000 km. Different wavelengths have been tested and plots are made below. Blue, green, red lines represent longer, current choice and shorter wavelengths.

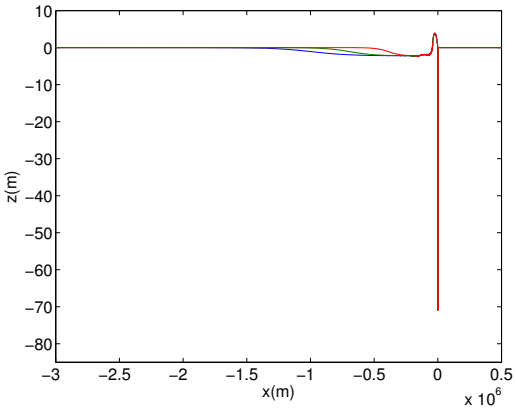

Figure 4.10: Time = 72000 s

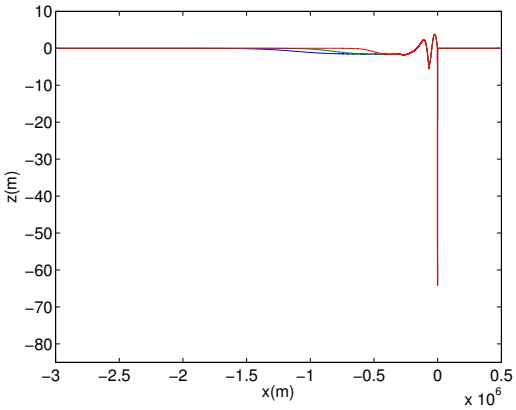

Figure 4.11: Time = 144000 s

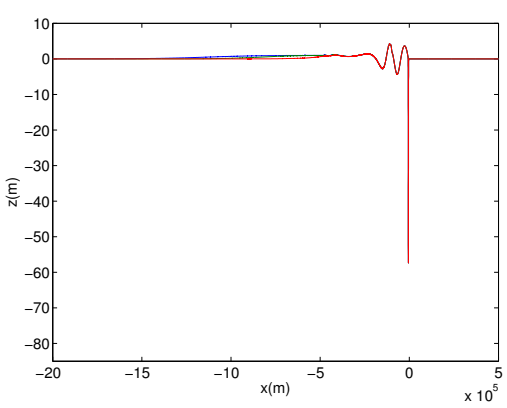

Figure 4.12: Time = 216000 s

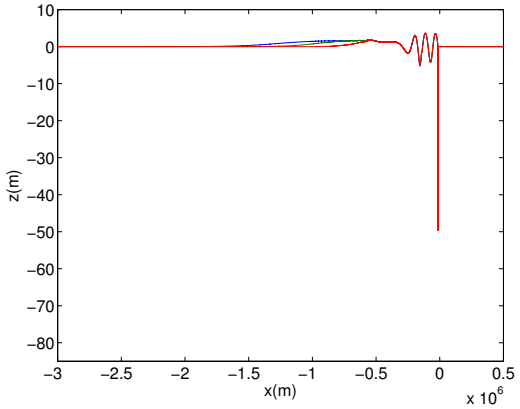

Figure 4.13: Time = 300000 s

It seems that as long as the wavelength is quite long, the difference in the wavlength of the elevation wave does not affect the shapes of the leading wave and the following solitary-like wave. The wave tail behinds all of the solitary-like small waves is slightly influenced. However, we are mostly interested in the leading wave profile and the changes of the following small waves. As a result, the current choice of the wavelength seems appropriate.

Stratification, Topography and Boundary Condition

The stratification used for this equation is exactly the same as that in the fully nonlinear model, and the bottom is flat. The boundary conditions in this model are

$$\eta_1 = \eta_2 = \eta_{I-1} = \eta_I = 0. \tag{4.18}$$

Numerical Method

All the coefficients in the equation are constant, since the water depth does not change. Both of the time and the space grids are uniform. We apply the finite difference method to our model equation. The trapezoidal rule is used for the integral.

$$\frac{\eta_n^{j+1} - \eta_n^{j-1}}{2dt} = -c_0 \frac{\eta_{n+1}^j - \eta_{n-1}^j}{2dx} - \alpha \eta_n^j \frac{\eta_{n+1}^j - \eta_{n-1}^j}{2dx} \tag{4.19}$$

$$-\alpha_1 (\eta_n^j)^2 \frac{\eta_{n+1}^j - \eta_{n-1}^j}{2dx} - \beta \frac{\eta_{n+2}^j - 2\eta_{n+1}^j + 2\eta_{n-1}^j - \eta_{n-2}^j}{2dx^3} \tag{4.20}$$

$$-\frac{f^2}{2} \cdot \frac{dt}{2} \sum_{m=0}^{j} (\eta_n^m + \eta_n^{m+1}) + \frac{f^2}{2c_0} \cdot \frac{dx}{2} \sum_{s=0}^{n} (\eta_s^0 + \eta_{s+1}^0) \tag{4.21}$$

where n, j are spatial and temporal indices.
As for the Ostrovsky solver, different resolutions have been used and compared. The details are provided in the next Chapter.

4.2.2 Ostrovsky equation solver

The model considered here is the integral form of the Ostrovsky equation, which is derived in Chapter 3. Here $[a, b]$ is the domain.

$$\eta_t + c_0\eta_x + \alpha\eta\eta_x + \beta\eta_{xxx} + \alpha_1\eta^2\eta_x = \frac{f^2}{2c}\Big(\int_a^x \eta dx' - \frac{1}{b-a}\int_a^b\int_a^x \eta(x',t)dx'dx\Big) \quad (4.22)$$

Solitary Wave Initialization

The initial condition $\eta(x, 0)$ shall satisfy these two conditions (3.90) and (3.91),

$$\int_a^b \eta(x', 0)dx' = 0, \quad (4.23)$$

$$\int_a^b\int_a^x \eta(x', 0)dx'dx = 0. \quad (4.24)$$

The initial wave profile contains four waves, two of which are solitary waves of depression and the other two are waves of elevation. The leading solitary wave is a solution of the eKdV equation, and the other three waves are small long waves which has the shape of $sech^2(x)$. The wave profile is plotted below.

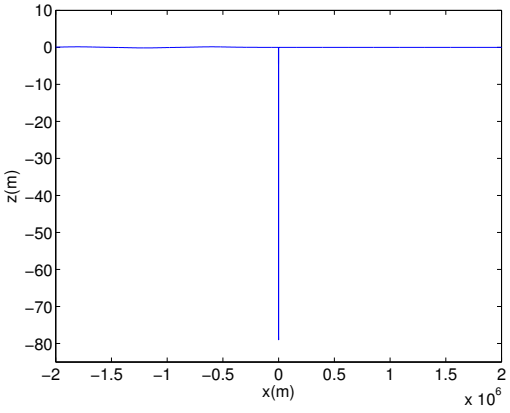

Figure 4.14: Initial wave profile for the Ostrovsky equation

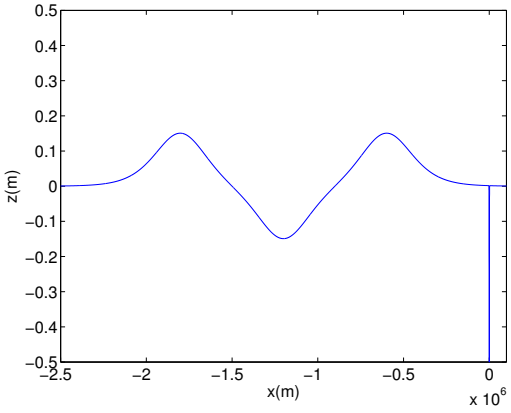

Figure 4.15: Zoomed in view of the initial elevation

Numerical Method

All the coefficients in the equation are constant, since the water depth does not change. Both of the time and the space grids are uniform. We apply the finite difference method to solve our model equation, which follows the method used in ([24]). The trapezoidal rule is used for the integral.

$$\frac{\eta_n^{j+1}-\eta_n^{j-1}}{2dt} = -c_0\frac{\eta_{n+1}^j-\eta_{n-1}^j}{2dx} - \alpha\eta_n^j\frac{\eta_{n+1}^j-\eta_{n-1}^j}{2dx} \tag{4.25}$$

$$-\alpha_1(\eta_n^j)^2\frac{\eta_{n+1}^j-\eta_{n-1}^j}{2dx} - \beta\frac{\eta_{n+2}^j-2\eta_{n+1}^j+2\eta_{n-1}^j-\eta_{n-2}^j}{2dx^3} \tag{4.26}$$

$$+\frac{f^2}{2c}\cdot\frac{dx}{2}\sum_{s=1}^{n}(\eta_s^j+\eta_{s+1}^j) \tag{4.27}$$

$$-\frac{f^2}{2c}\cdot\frac{1}{b-a}\frac{dx}{2}\sum_{m=1}^{N_x}\Big(\frac{dx}{2}\sum_{s=1}^{m}(\eta_s^j+\eta_{s+1}^j)+\frac{dx}{2}\sum_{s=1}^{m+1}(\eta_s^j+\eta_{s+1}^j)\Big) \tag{4.28}$$

where n, j are spatial and temporal indices. N_x is the number of the grid points in the x direction.

Resolution tests were done using different grid sizes and time steps to ensure the solutions were adequately resolved. Details are provided in the next chapter.

Chapter 5

Simulation Results

5.1 Resolution Test

All of the model tests use initial waves of amplitudes = 79 m. Smaller waves are not tested. The water depth is set to be 500 m.

5.1.1 IGW model

One set of simulations has been run to find the appropriate dx and dt. The first set includes one case using a low resolution, i.e., dx=20 m and dt=2.5 s. The high resolution uses dt = 1.5 s and dx = 20 m. The plot at time = 0 s is omitted. Figure (5.1) compares the wave profile from the low and the high resolution. The plot on the left is a general look of the whole wave profile, and the plot on the right is zoomed in for the amplitudes.

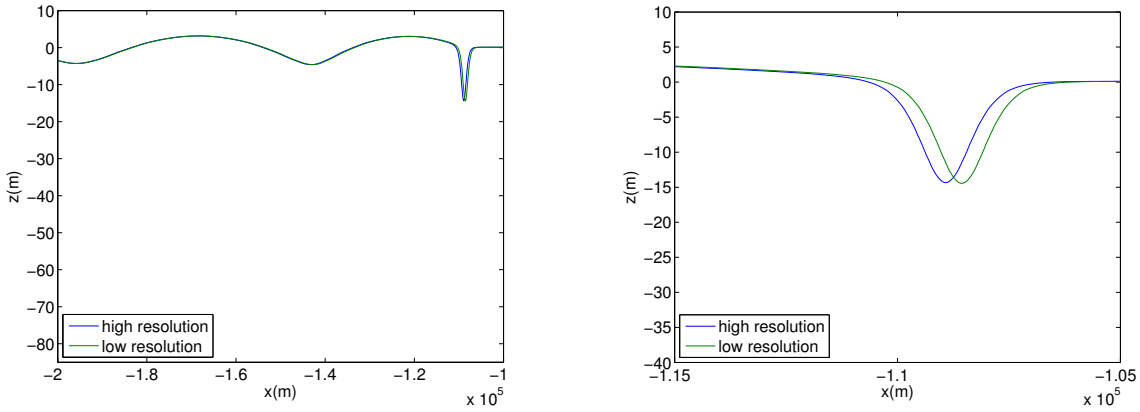

Figure 5.1: Time = 600000 s. Results are from IGW simulation. Initial wave amplitude is 79 m, and the plots show the vertical displacement of a isopycnal where the displacement is the greatest.

The difference between the shapes of the wave trains and the leading wave amplitudes are very small. The difference in the position of the wave crests is approximately 500 m, which gives an error of 0.04% calculated by $\frac{|\text{difference of propagation distance}|}{\text{total propagation distance}}$. It will be shown later the differences between IGW and the two weakly nonlinear models are $D_O = 0.89\%$ and $D_{AO} = 2.6\%$. Hence, it indicates that the choice of temporal step in the low resolution case is appropriate.

5.1.2 Ostrovsky Solver

Two simulations have been run to find the appropriate dx and dt. One case uses a low resolution, i.e., dx=50 m and dt=0.025 s. The other case uses a high resolution, and I choose dx=32 m and dt=0.016 s. Figures (5.2) and (5.3) show plots of the wave profiles at the final time for the Ostrovsky solver. The initial wave profile at time = 0 s is omitted. The plot on the left is a general look of the whole wave profile. The plot on the right is zoomed in order to see the details of the amplitudes.

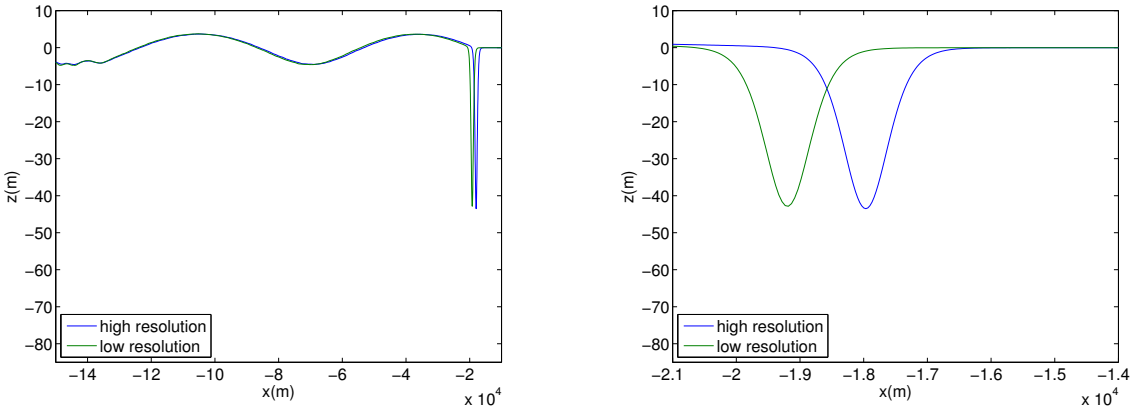

Figure 5.2: Time = 300000 s for the Ostrovsky solver. Plots show the vertical displacement of the isopycnal.

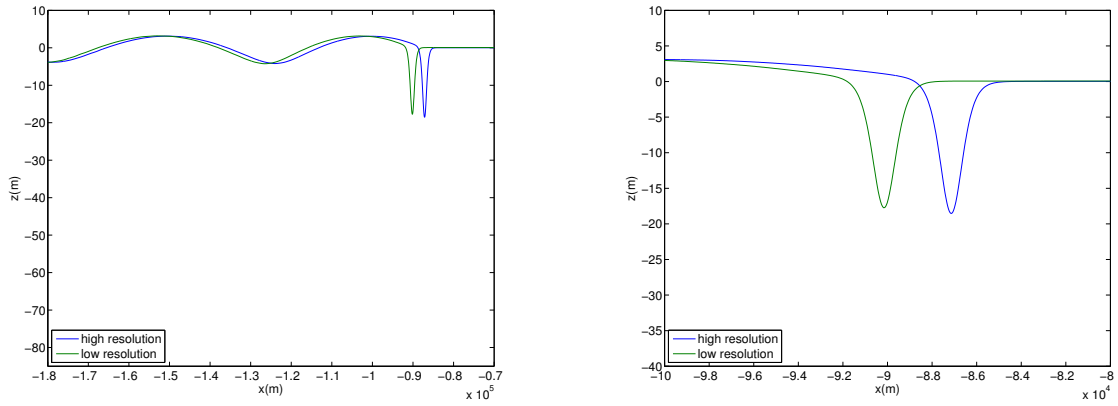

Figure 5.3: Time = 600000 s for the Ostrovsky solver. Plots show the vertical displacement of the isopycnal.

From the plots we can see that the shape of the wave train is almost the same. The amplitude difference is very small as well. The difference between the two wave crests are around 2750 m and the total propagation distance is around 1.4e6 m. The difference is about 0.20%, which is very small. This shows that the choice of spatial and time steps in the low resolution are appropriate.

5.1.3 Alternative Ostrovsky Solver

All the choices of the spatial and the time steps are the same as that in the Ostrovsky solver. Details are omitted here. Below are some plots of the wave profiles at different time steps for the alternative Ostrovsky solver. The plot on the left is a general look of the whole wave profile. The plots on the right are zoomed in for the amplitudes.

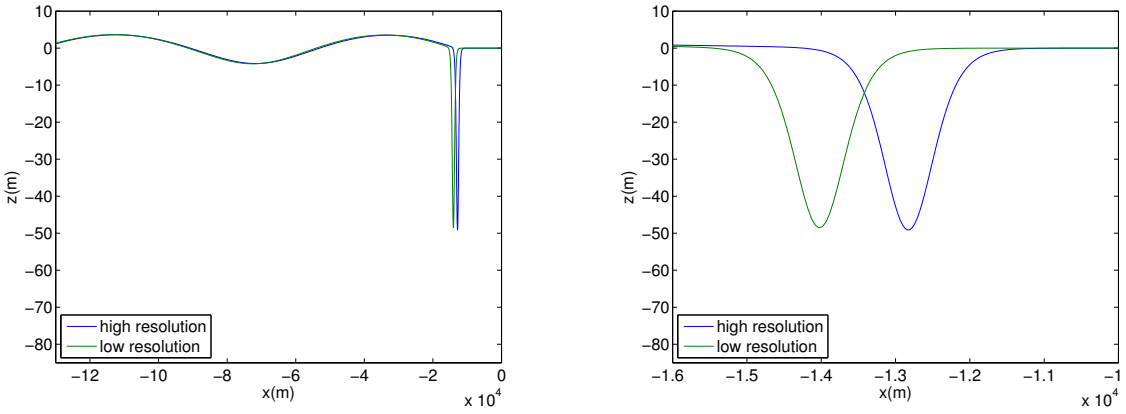

Figure 5.4: Time = 300000 s for the alternative Ostrovsky solver.

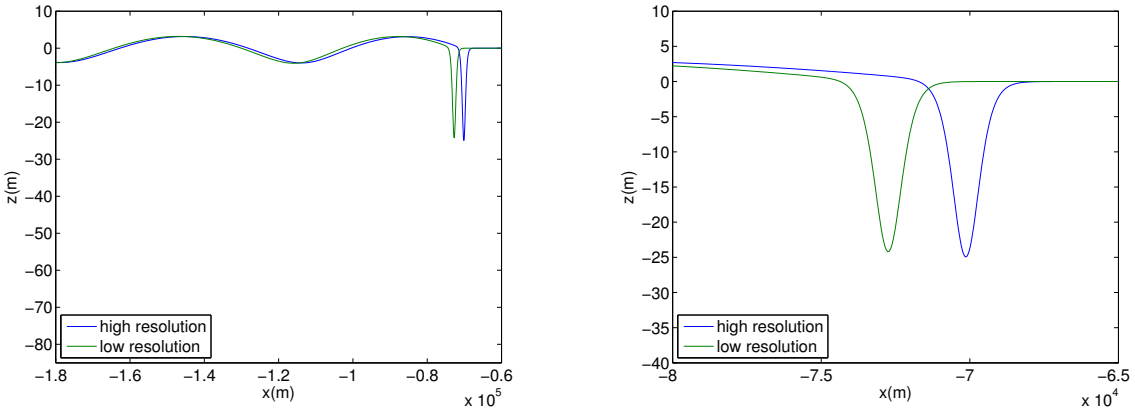

Figure 5.5: Time = 600000 s for the alternative Ostrovsky solver.

From the plots we can see that the shape of the wave train is almost the same. The amplitude difference is very small as well. The difference between the two wave crests are around 2500 m and the total propagation distance is around 1.4e6 m. The difference is about 0.18%, which is very small. This shows that the choice of spatial and time steps in the low resolution are appropriate.

5.2 Comparisons of IGW, Ostrovsky and alternative Ostrovsky equations

Simulations with three different initial wave amplitudes have been run and compared. Besides the difference in the wave amplitudes, all the other variables are the same in the following simulations. The water depth is set to be 500 m.

5.2.1 Amplitude = 79 m

Figures (5.6) to (5.11) are plots of the wave profile at different times. I have shifted the reference frame so that the moving frame moves with the linear long wave propagation speed. For the weakly nonlinear models, only the leading wave is shown.

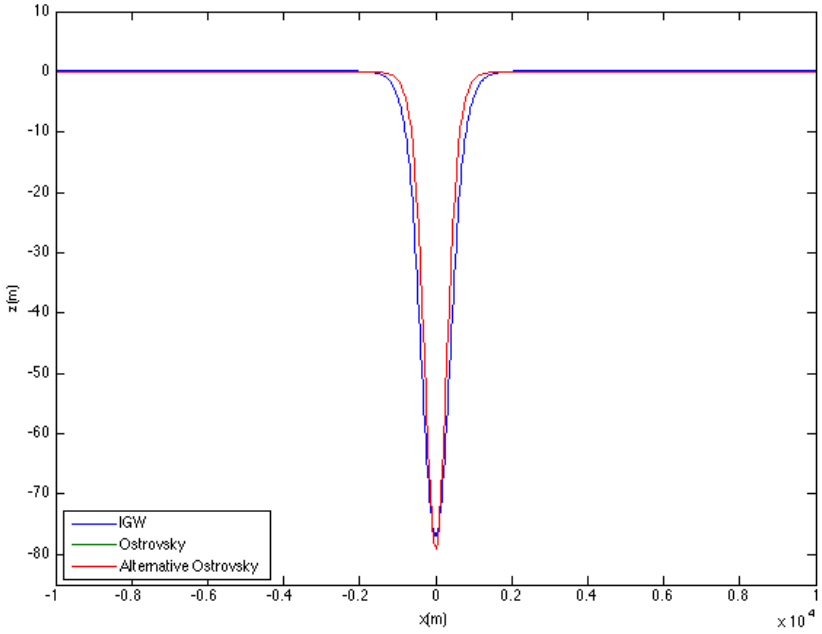

Figure 5.6: Time = 0s. The initial leading wave profile of Ostrovsky and alternative Ostrovsky solvers are exactly the same, so they coincide with each other. The initial waves of the IGW and the weakly nonlinear models are slightly different, since IGW uses solitary wave solution of the DJL equation not the eKdV equation.

Each set of the plots below is at a fixed time. The plot on the left is a general look of the whole wave profile. The plot on the right is a zoom for the amplitudes.

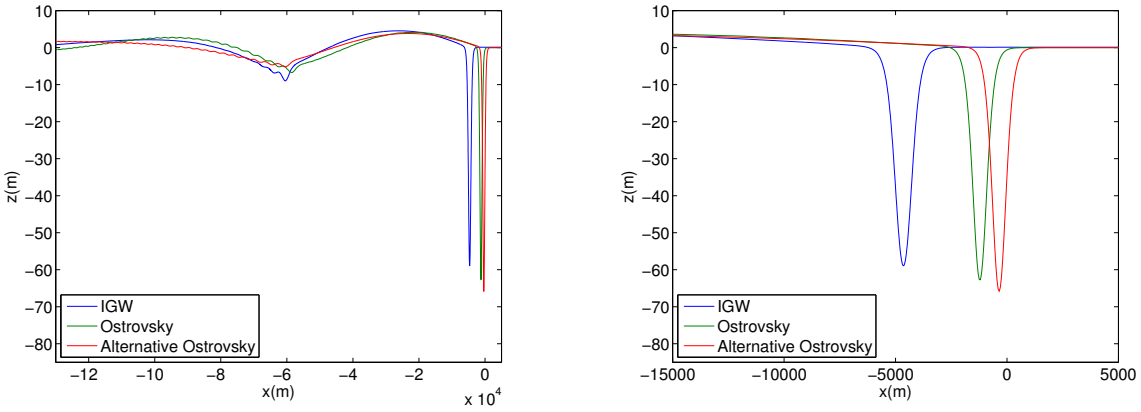

Figure 5.7: Time = 120000 s.

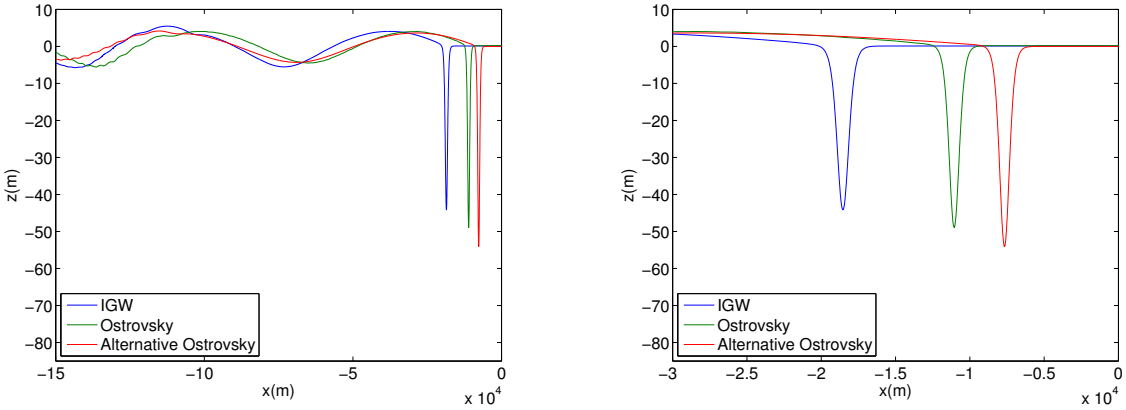

Figure 5.8: Time = 240000 s.

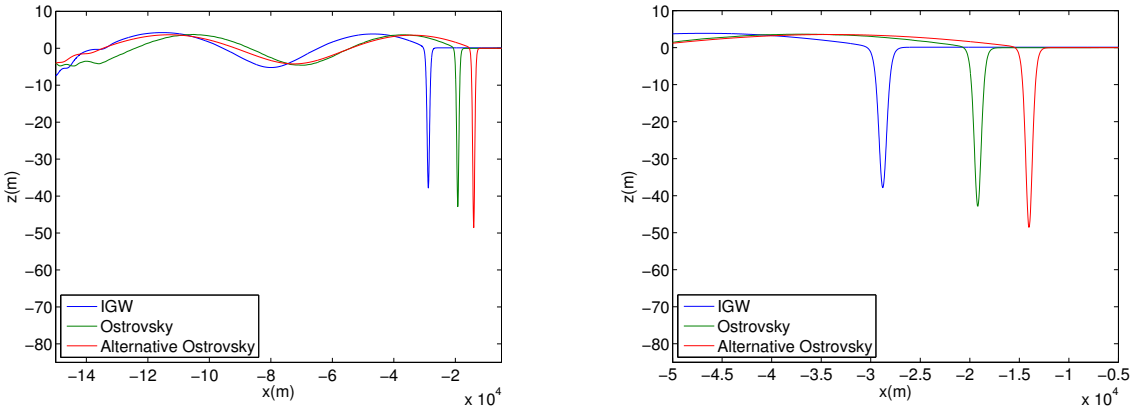

Figure 5.9: Time = 300000 s.

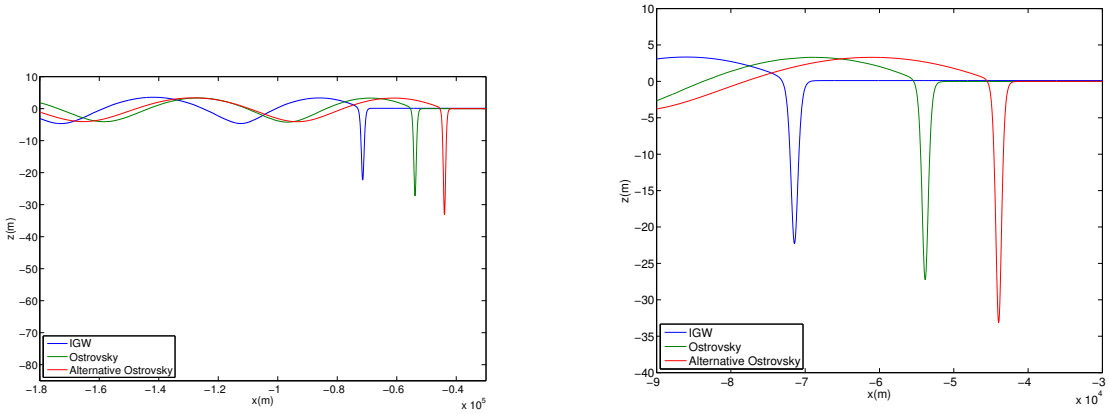

Figure 5.10: Time = 480000 s.

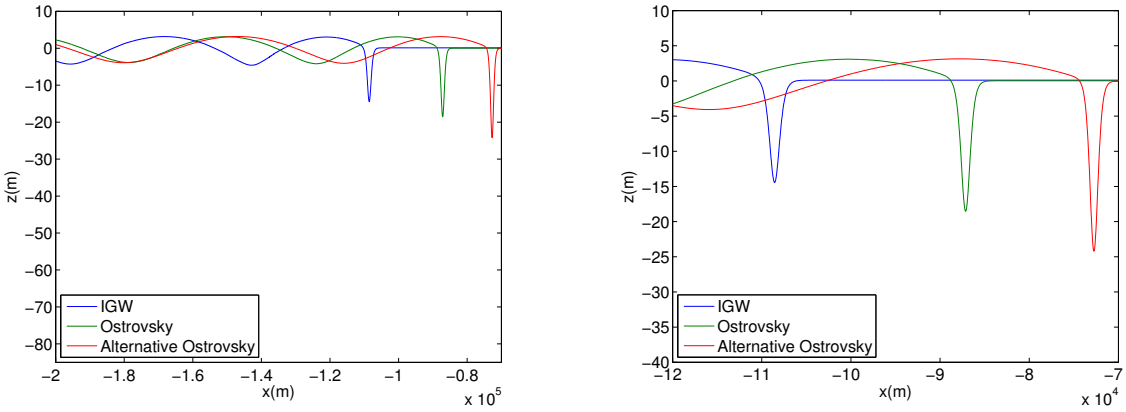

Figure 5.11: Time = 600000 s.

As time increases, all three models gives similar predictions of the shape of the wave train. At the final time, the wavenumber of the long wave trains predicted by each model is k_{igw} = 1.4e-4 m^{-1} (for IGW), k_O = 1.3e-4 m^{-1} (for Ostrovsky) and k_{AO} = 1.1e-4 m^{-1} (for Alternative Ostrovsky). The wavenumber keeps changing during the propagation. For example, at time t = 300000 s, k_{igw} = 9.67e-5 m^{-1}, k_O = 8.98e-5 m^{-1} and k_{AO} = 7.85e-5 m^{-1}. The wavenumber increases from t = 3e5 s to t = 6e5 s.
The amplitudes predicted by the weakly nonlinear models are larger than that by the IGW. If we use the amplitude of the IGW as the standard, at the final time, the errors of the leading wave amplitudes from the two weakly nonlinear models are, A_O = 20.7% and A_{AO} = 65.5% larger, which are calculated as $A = \frac{|a_{weak} - a_{igw}|}{a_{igw}}$. The table below shows the decaying process of the leading wave for each model.

Table 5.1: The amplitude decay of the leading wave

	time for wave decaying to 50%	time for wave decaying to 25 %	at t = 6e5 s, $(\frac{\text{wave amplitude}}{\text{initial amplitude}}) \times 100\%$
IGW	276000 s	504000 s	18 %
Ostrovsky	324000 s	564000 s	22 %
Alternative Ostrovsky	396000 s	N/A	30 %

The weakly nonlinear models propagate faster than the IGW. At t = 600000 s, the errors of propagation distances are, D_O = 0.89% and D_{AO} = 2.6% faster, which is calculated as

$$D = \frac{|d_{weak} - d_{IGW}|}{total\ propagation\ distance}. \tag{5.1}$$

5.2.2 Amplitude = 43 m

Below are plots of the wave profile at different times. Similar to the analogy in the previous subsection, I have shifted the reference frame so that the frame moves with the linear long wave propagation speed. For the weakly nonlinear models, only the leading wave is shown.

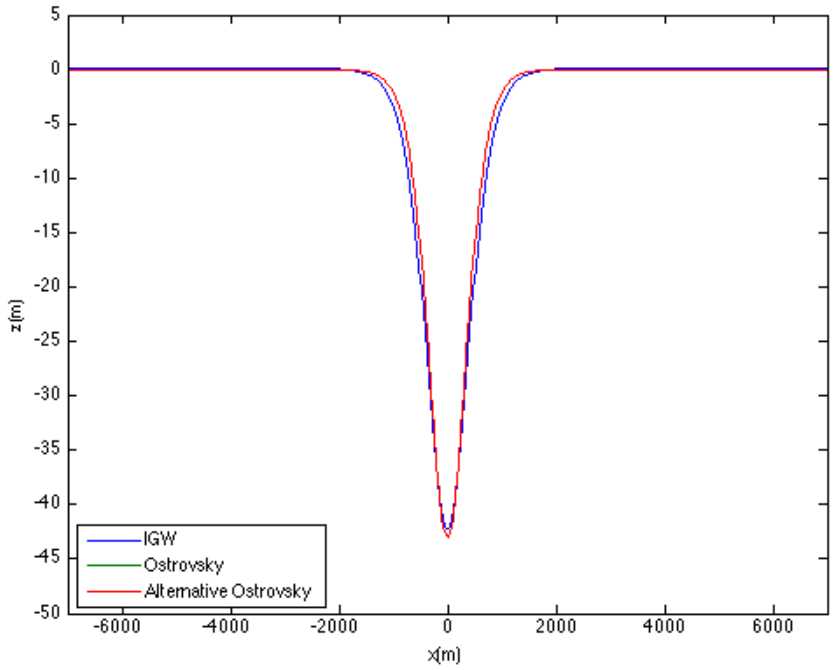

Figure 5.12: Initial wave profile

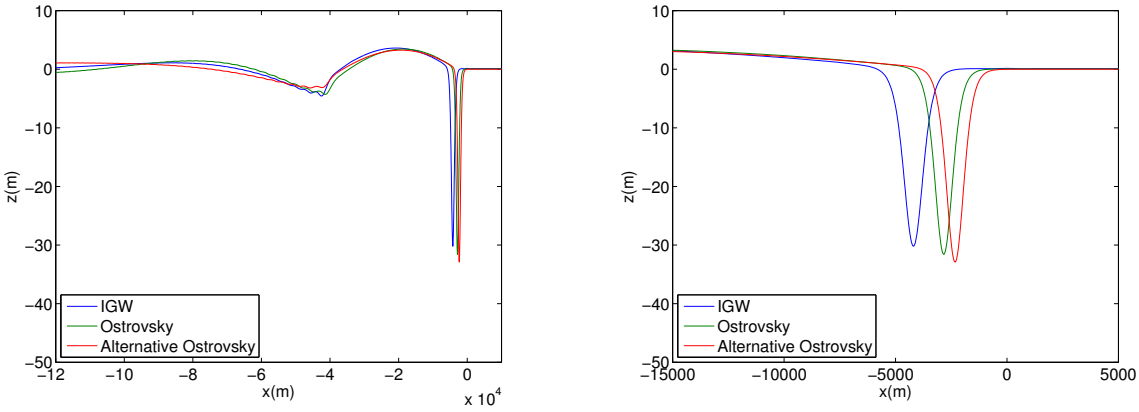

Figure 5.13: Time = 120000 s.

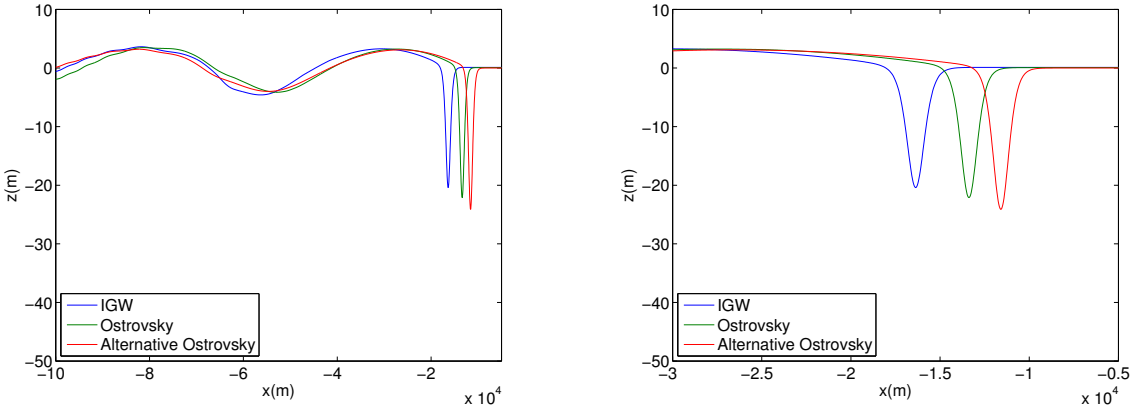

Figure 5.14: Time = 240000 s.

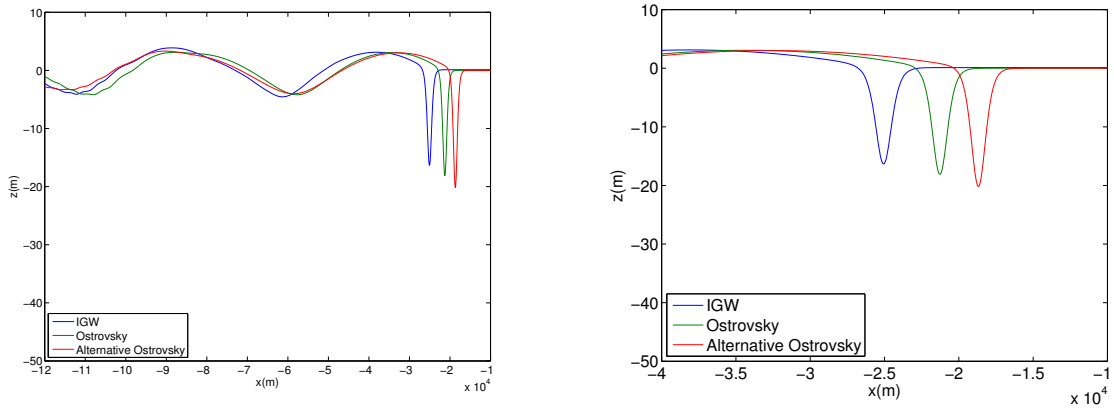

Figure 5.15: Time = 300000 s.

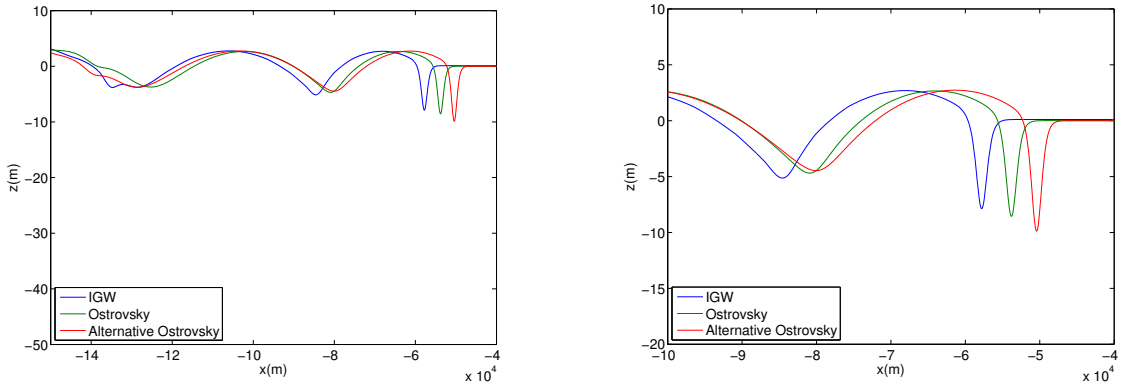

Figure 5.16: Time = 480000 s.

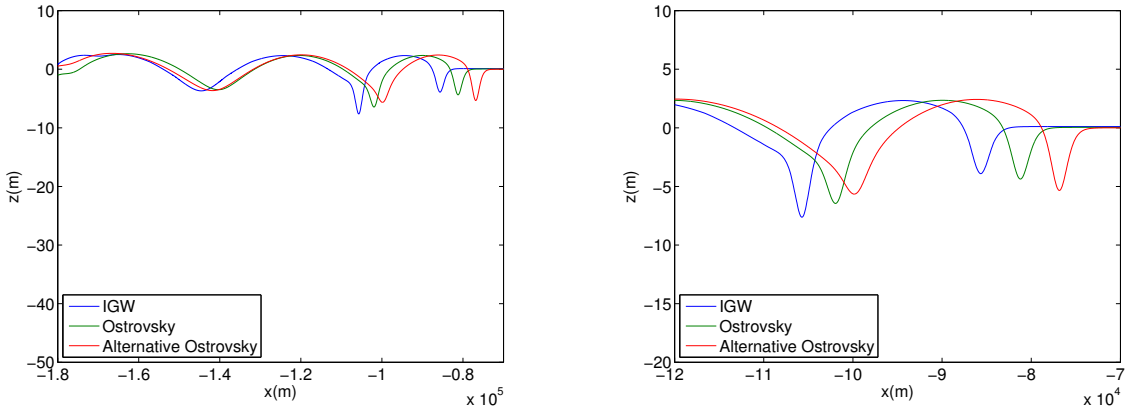

Figure 5.17: Time = 600000 s.

All of the three models gives similar predictions of the shape of the wave train. At the final time, the wavenumbers of the long wave trains given by each model are slightly different, where k_{igw} = 2.2e-4 m^{-1}, k_O = 2.2e-4 m^{-1} and k_{AO} = 1.9e-4 m^{-1}. The wavenumber keeps changing during the propagation process. For example, at t = 3e5 s, the wavenumbers given by each model are, k_{igw} = 1.3e-4 m^{-1}, k_O = 1.2e-4 m^{-1} and k_{AO} = 1.1e-4 m^{-1}. The wavenumber increases from t = 3e5 s to t = 6e5 s for all models.
The errors of the leading wave amplitudes from the two weakly nonlinear models are, A_O = 12.5% and A_{AO} = 37.5%. The table below shows the decaying process of the leading wave for each model.

Table 5.2: The amplitude decay of the leading wave

	time for wave decaying to 50%	time for wave decaying to 25 %	at t = 6e5 s, $\left(\frac{\text{wave amplitude}}{\text{initial amplitude}}\right) \times 100\%$
IGW	240000 s	408000 s	8.4 %
Ostrovsky	264000 s	432000 s	9.3 %
Alternative Ostrovsky	276000 s	468000 s	12 %

At the final time, the errors of propagation distance are, D_O = 0.4% and D_{AO} = 0.96%.

5.2.3 Amplitude = 23 m

Below are plots of the wave profile at different times. Similar to the analogy in the previous subsections, I have shifted the reference frame so that the moving frame moves with the

linear long wave propagation speed. For the weakly nonlinear models, only the leading wave is shown.

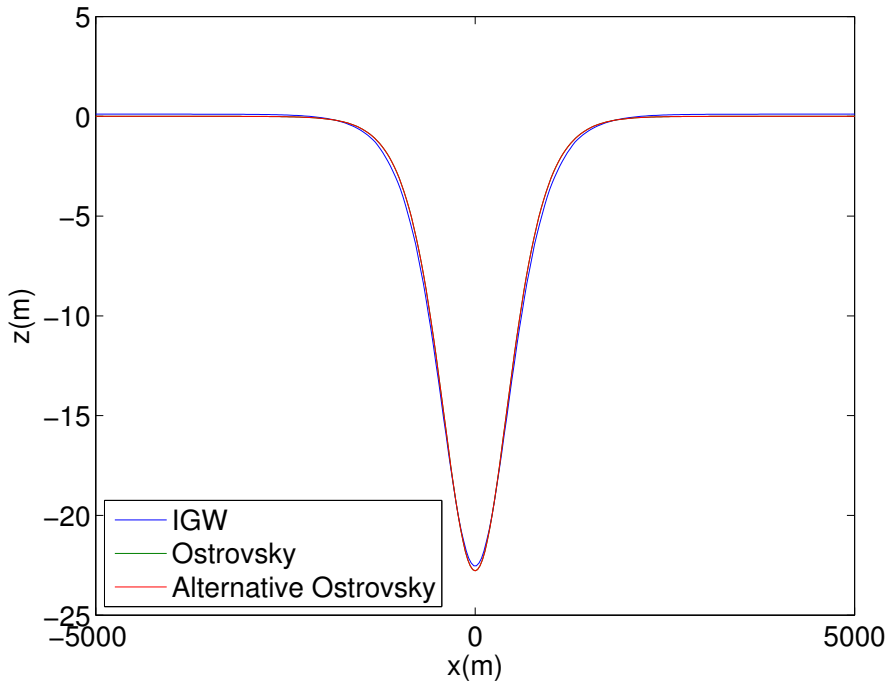

Figure 5.18: Initial wave profile

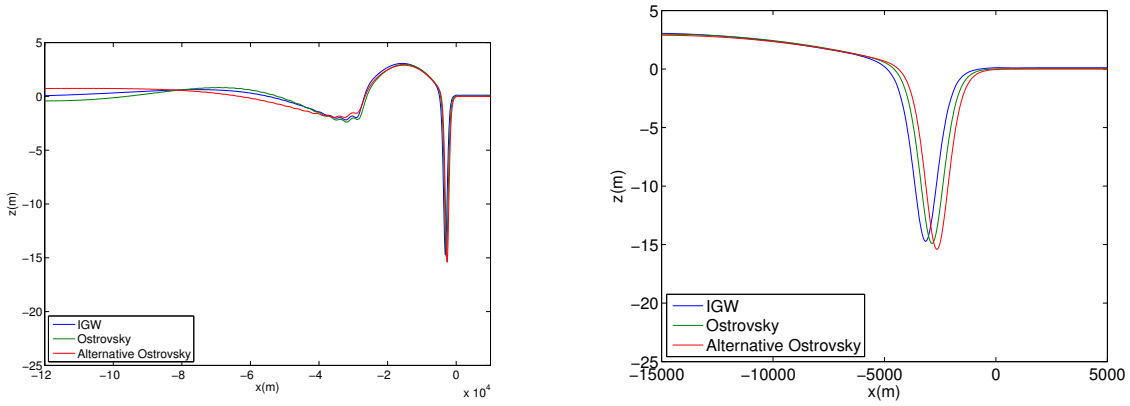

Figure 5.19: Time = 120000 s.

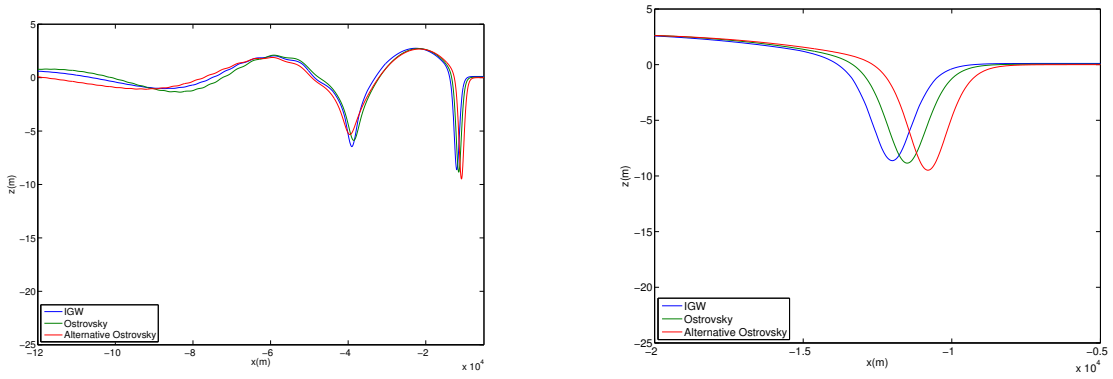

Figure 5.20: Time = 240000 s.

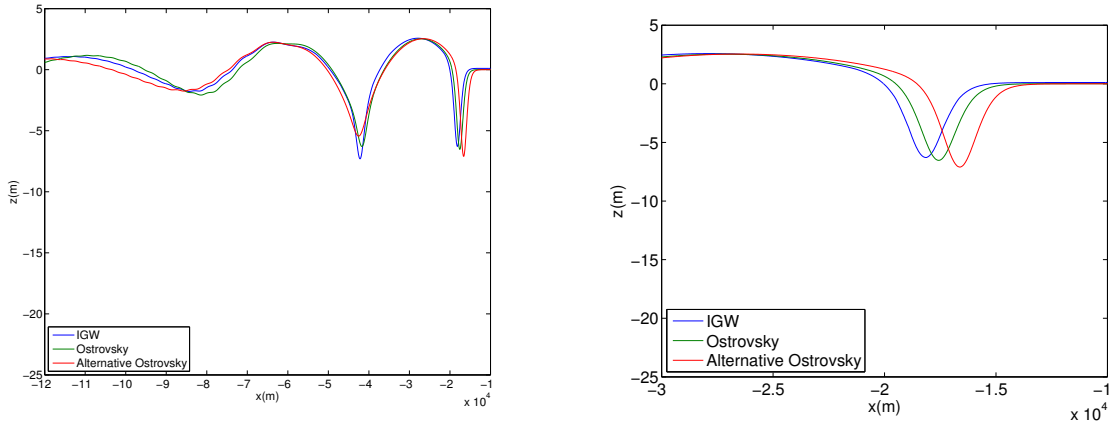

Figure 5.21: Time = 300000 s.

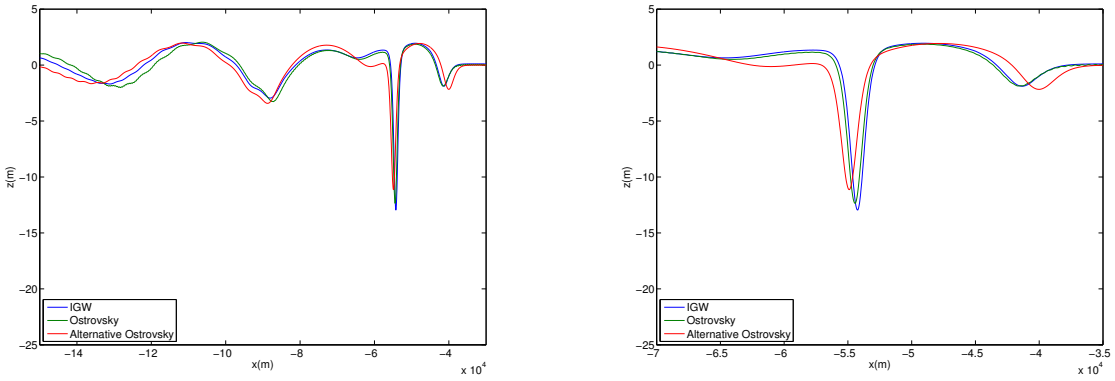

Figure 5.22: Time = 480000 s.

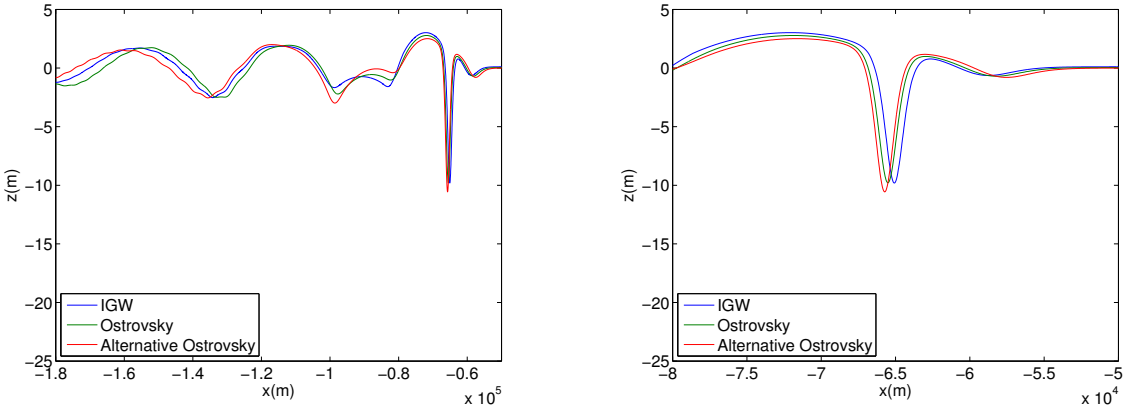

Figure 5.23: Time = 600000 s.

All of the three models gives similar predictions of the shape of the wave train. At the final time, the wavenumber is difficult to measure and the leading wave is hardly observable from the plots. Instead, the second solitary-like wave is very clearly formed. The table below shows the decaying process of the leading wave for each model.

Table 5.3: The amplitude decay of the leading wave

	time for wave decaying to 50%	time for wave decaying to 25 %	time for wave decaying to 10 %	at t = 6e5 s, $\left(\frac{\text{wave amplitude}}{\text{initial amplitude}}\right)\times$ 100%
IGW	180000 s	312000 s	432000 s	2.6 %
Ostrovsky	180000 s	324000 s	456000 s	2.6 %
Alternative Ostrovsky	192000 s	336000 s	468000 s	3.4 %

From these three different simulation results, we can see that both of the weakly nonlinear models manage to capture the changing behavior of the ISW while propagating with Earth' rotation. The addition of the rotation term breaks the balance between the nonlinear effects and the dispersive effect. The energy is slowly diverted from the leading wave to the wave train behind it. The nonlinear effects help the wave tail of the leading wave to steepen up, thus form a smaller solitary-like wave behind it. Then the second solitary-like wave is formed in a similar way, followed by the first solitary-like wave. These different solitary-like waves have different wavelengths, and they all propagate in different speeds due to the dispersive effects. If we take the results from IGW as the reference, the leading wave amplitudes and the propagation speeds predicted by the Ostrovsky solver match better with the IGW than that from the alternative Ostrovsky solver. Hence, the Ostrovsky equation seems to give a better performance.

Comparing the results from the three sets of simulation, we can see that, as the amplitude of the initial wave decreases, the differences among the three models decreases and the weakly nonlinear models become more accurate. This is reasonable since the weakly nonlinear models are derived based on the assumption that the wave amplitude is very small.

5.3 Simulation Analysis

The three models have predicted different wavelengths of the long wave tails, amplitudes and propagation speed of the leading waves. To analyze these different results, plots of frequencies, phase speeds and group velocities have been made from the linearized version of these three models. All the coefficients used in the plots are obtained from the corresponding numerical simulations.

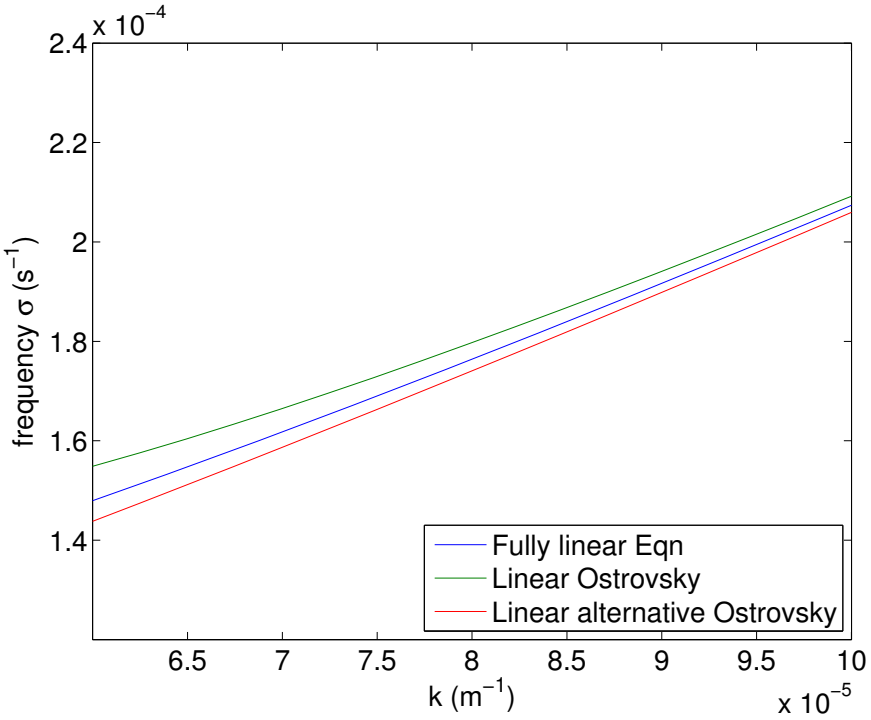

Figure 5.24: Frequency vs wavenumber for the linearized equations. A small range of k values are plotted here, since only these values will be needed in the later analysis.

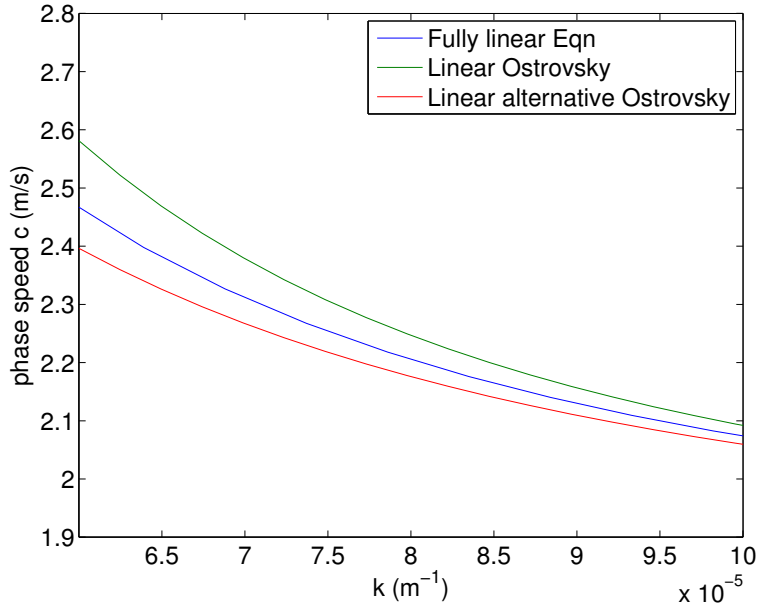

Figure 5.25: Phase speed vs wavenumber for the linearized equations.

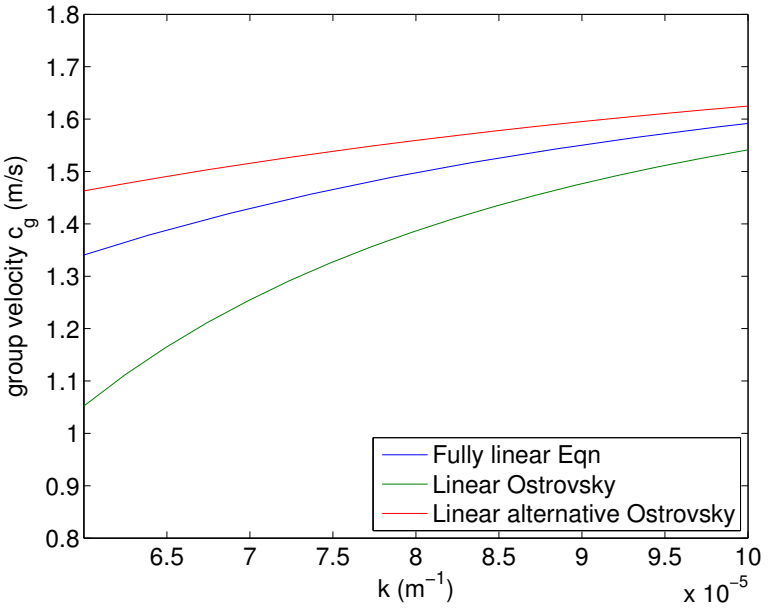

Figure 5.26: Group velocity vs wavenumber for the linearized equations.

When the amplitude of the initial wave is 79 m and at t = 300000 s, the wavenumbers of the long wave trains for each model are k_{igw} = 9.67e-5 m^{-1}, k_O = 8.98e-5 m^{-1} and k_{AO} = 7.85e-5 m^{-1}, which we can get from the previous section. From the plots made above, we can see that the phase speeds of the three models are very close. The phase speed of the linearized alternative Ostrovsky (LAO) equation is the fastest, then followed by linearized Ostrovsky (LO) and fully linear (LF) equations, which matches the simulation results.

Combining the plots of phase speeds and the plots of group velocities, we can get the velocity of the wave train relative to the leading wave propagation speed. We name this velocity of the wave train as Δ_c, which is calculated by $\Delta c = |c - c_g|$. The larger Δc is, the more rapidly the energy is drained from the leading wave. Since this will decrease the amplitude of the leading wave, and decrease the wave propagation speed, the larger the Δc is, the slower the wave propagates. As such, we would expect $\Delta c_{LAO} < \Delta c_{LO} < \Delta c_{LF}$, since $c_{LAO} > c_{LO} > c_{LF}$. However, the data we get from the plots of the linearized equations do not support this result.
The two other cases with amplitudes = 43 m and 23 m give the similar results. The plots are omitted here, and all the data is listed below.

Table 5.4: amplitude = 79m

	LF	LO	LAO
phase speed c (m/s)	2.09	2.15	2.19
group velocity c_g (m/s)	1.58	1.49	1.55
Δc (m/s)	0.51	0.66	0.64

Table 5.5: amplitude = 43m

	LF	LO	LAO
phase speed c (m/s)	1.97	2.01	2.02
group velocity c_g (m/s)	1.68	1.63	1.65
Δc (m/s)	0.29	0.38	0.37

Table 5.6: amplitude = 23m

	LF	LO	LAO
phase speed c (m/s)	1.891	1.893	1.898
group velocity c_g (m/s)	1.745	1.739	1.741
Δc (m/s)	0.146	0.154	0.157

As the amplitude of the initial wave decreases, the phase speeds of all the models decrease. At the same time, the phase speeds of the leading solitary wave predicted by all the models get closer, which is consistent with the simulation results. This is expected since the weakly nonlinear models perform better with smaller amplitude waves. This can also be explained by the changes of the wavenumber k. Simulation results indicate that k increases as the amplitude of the initial wave decreases, and figure (5.27) below shows, for $k \in$ [6e-5, 5e-4] m^{-1}, the phase speeds of all linearized models decrease and converge to the linear long wave speed as k increases. Figures (5.28) and (5.29) show similar results with the group velocities and the frequencies.

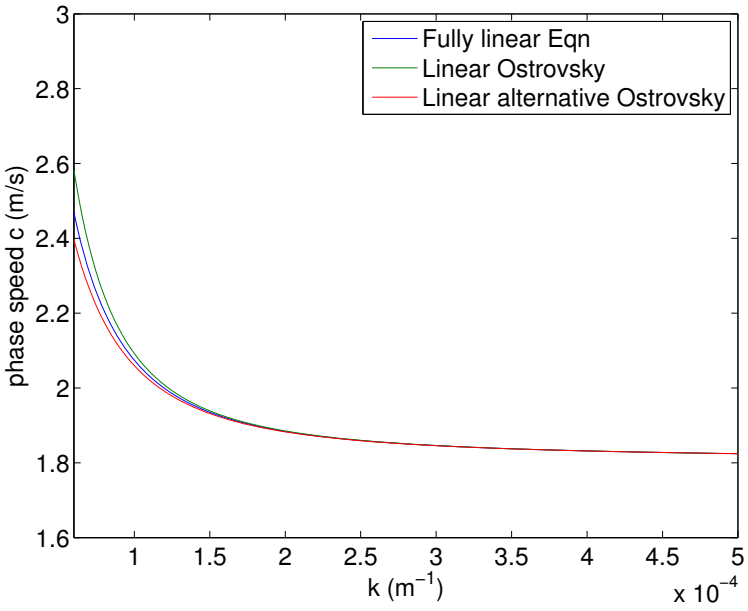

Figure 5.27: Phase speed vs wavenumber for the linearized equations.

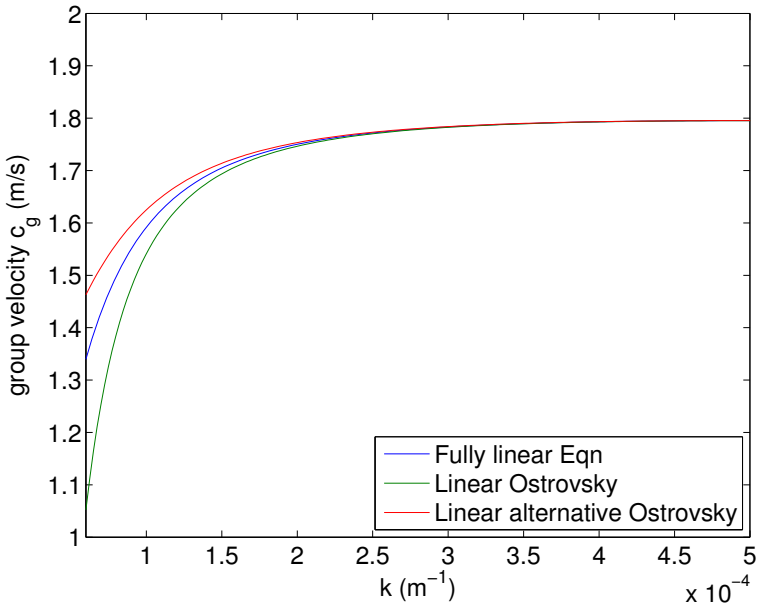

Figure 5.28: Group velocity vs wavenumber for the linearized equations.

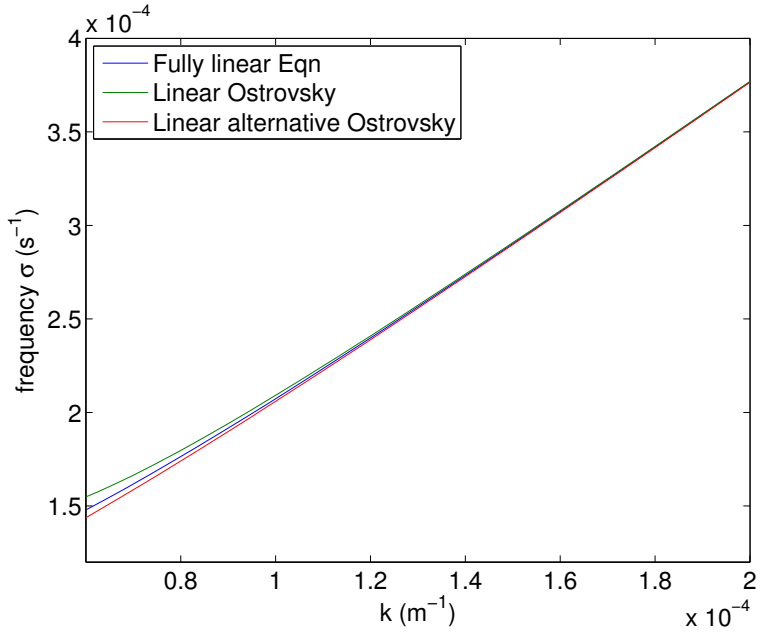

Figure 5.29: Frequency vs wavenumber for the linearized equations. A smaller range for k, i.e. [6e-5, 2e-4] m^{-1}, is plotted here to have a clear view to the changes of the frequencies.

Figures (5.30) to (5.32) below show the changes of σ, c and c_g with wider ranges of k. Figure (5.33) shows the behavior of $|c - c_g|$ with different ranges of k.

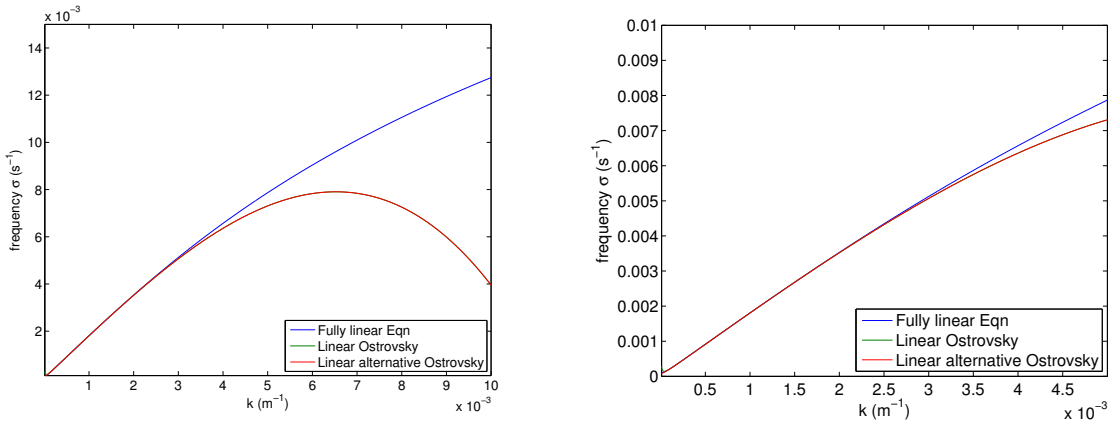

Figure 5.30: Frequency vs wavenumber for the linearized equations. The plot on the left has a range of k as [1e-5, 1e-2] m^{-1}; the plot on the right has a range of k as [1e-5, 5e-3] m^{-1}. The plots for LO are not observable since they almost coincide with the plots for LAO.

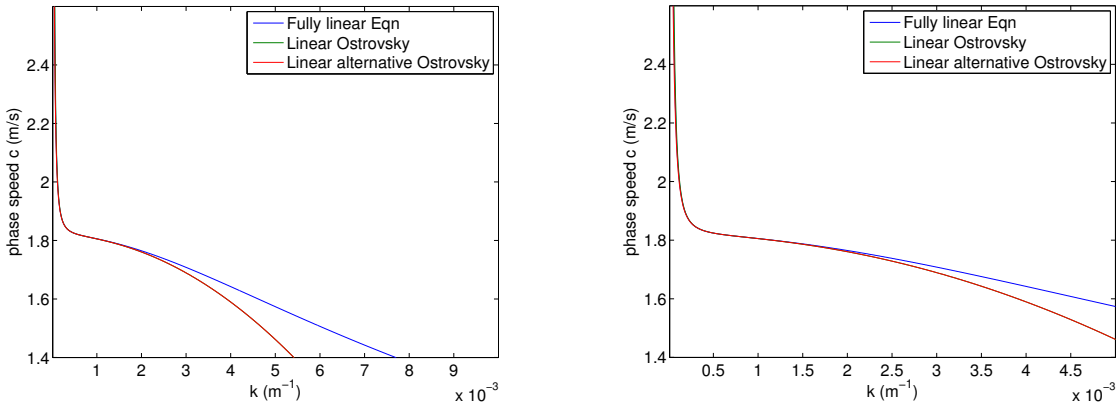

Figure 5.31: Phase speed vs wavenumber for the linearized equations. The plot on the left has a range of k as [1e-5, 1e-2] m^{-1}; the plot on the right has a range of k as [1e-5, 5e-3] m^{-1}. The plots for LO are not observable since they almost coincide with the plots for LAO.

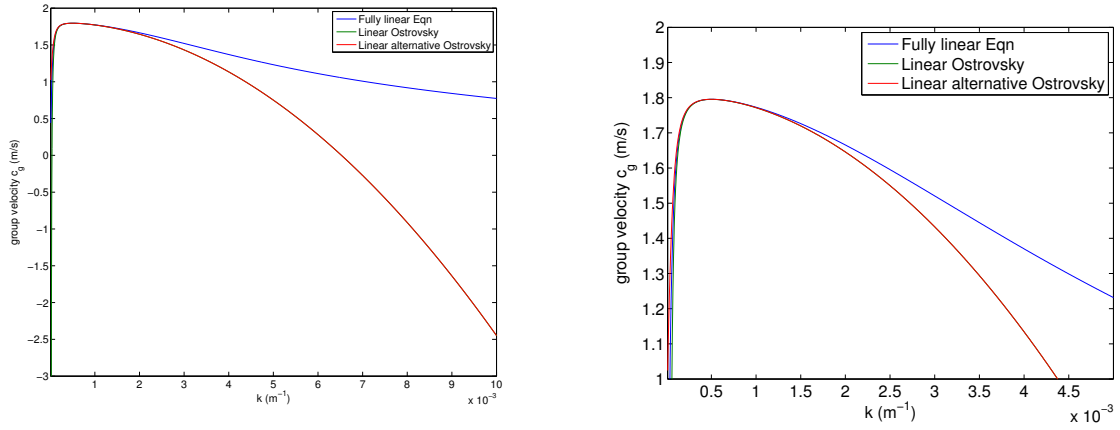

Figure 5.32: Group velocity vs wavenumber for the linearized equations. The plot on the left has a range of k as [1e-5, 1e-2] m^{-1}; the plot on the right has a range of k as [1e-5, 5e-3] m^{-1}. The plots for LO are not observable since they almost coincide with the plots for LAO.

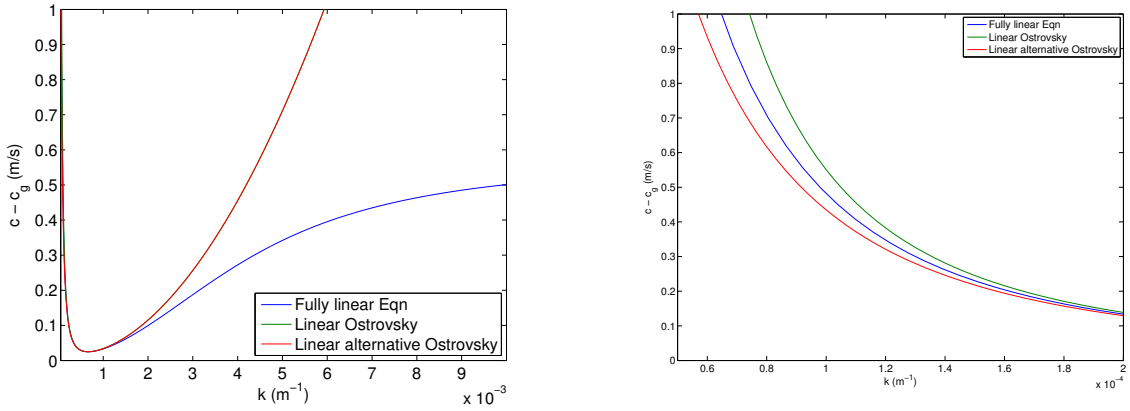

Figure 5.33: $|c - c_g|$ vs wavenumber for the linearized equations. The plot on the left has a range of k as [1e-5, 1e-2] m^{-1}; the plot on the right has a range of k as [1e-5, 2e-4] m^{-1}. The plot for LO on the left hand side is not observable since it almost coincides with the plot for LAO.

Figures (5.29) and (5.30) indicate that the frequencies of the three models match the best when $k \in$ [1.2e-4, 2.5e-3] m^{-1}; figures (5.27) and (5.31) indicate that the phase speeds of the three models match the best when $k \in$ [2e-4, 2e-3] m^{-1}; figures (5.28) and (5.32) indicate that the group velocities of the three models match the best when $k \in$ [2.5e-4,

1.2e-3] m^{-1}, which is also the range for k when $|c - c_g|$ matches the best. These suggest that when $k \in$ [2.5e-4, 1.2e-3] m^{-1}, the weakly nonlinear models perform the best given the current stratification and water depth.
At t = 3e5 s, table (5.3) shows the wavenumer k of the long wave trains for all the models.

Table 5.7: Wavenumber k for different models at t = 3e5 s.

	IGW	Ostrovsky	Alternative Ostrovsky
Amplitude = 79 m	9.67e-5 m^{-1}	8.98e-5 m^{-1}	7.85e-5 m^{-1}
Amplitude = 43 m	1.3e-4 m^{-1}	1.2e-4 m^{-1}	1.1e-4 m^{-1}
Amplitude = 23 m	1.9e-4 m^{-1}	1.9e-4 m^{-1}	1.8e-4 m^{-1}

As the amplitude of the initial wave decreases, the difference of k in the three simulations decreases and for each model, k increases and approaches the best performance range [2.5e-4, 1.2e-3] m^{-1}. This supports the fact that the weakly nonlinear models work better when the amplitude of the initial wave is smaller. In addition, the weakly nonlinear models may perform better as the amplitude decreases further.
However, the best range of k for $|c - c_g|$ is much smaller than that for c, and all the k values in the table, though they are approaching, have not reached the range for $|c - c_g|$. This probably explains why this analysis fails to show that $\Delta c_{LAO} < \Delta c_{LO} < \Delta c_{LF}$, while it manages to show $c_{LAO} > c_{LO} > c_{LF}$.

Chapter 6

Conclusion

6.1 Summary

In this thesis, a new equation, alternative Ostrovsky equation, derived by Lamb ([33]), is introduced to model the behavior of ISWs with the Earth's rotation. Following the derivation of the alternative Ostrovsky equation, the derivation of the Ostrovsky equation has been briefly described. Two weakly nonlinear models, Ostrovsky and alternative Ostrovsky solvers, are used in the numerical simulations. Here the alternative Ostrovsky solver has been modified from the existing Ostrovsky solver. Finite difference method up to second-order accuracy is adopted in both of these two solvers. Solitary wave solutions from Gardner equation are used as the initialization. Simulation results from the Ostrovsky and alternative Ostrovsky solvers are compared with the two-dimensional fully nonlinear model, i.e., IGW, to investigate the validity of the weakly nonlinear models. IGW uses solutions from DJL equation as the initial wave profile, and second-order projection method is used as the numerical method.

In all of the numerical simulations, the water depth is set to 500 m and the bottom is flat. The stratification is an analytic expression given in (4.9). The thermocline lies between water depth of 55 m and 120 m. We have run three sets of numerical simulations with initial wave amplitudes of 79 m, 43 m and 23 m. The time span of each simulation is 600000 s, and the Coriolis parameter is taken as 10^{-4} rad/s, which is a typical value for mid-latitudes. Resolution tests have been run for each model to determine the appropriate spatial and the temporal steps.

Based on the simulation results in the thesis, the Ostrovsky equation provides better predictions of the leading wave amplitudes and the propagation speeds than the alternative Ostrovsky equation. As the initial wave amplitude decreases, the differences be-

tween the weakly nonlinear models also decrease. This agrees with the assumption of the weakly nonlinear models, i.e., $\epsilon \approx \frac{a}{H} \ll 1$. In addition, as the initial wave amplitude decreases, the wavenumber of each model increases and the wavelength decreases. This also agrees with the assumption of the weakly nonlinear models that, $\mu = (\frac{H}{L})^2 \ll 1$ and $\delta = \frac{f^2L^2}{c^2} = \frac{f^2L^2}{N^2H^2} \ll 1$, which suggests $H^2 \ll L^2 \ll \frac{N^2H^2}{f^2}$. The weakly nonlinear models perform well when the wavelength is long but not too long since the rotational effects are assumed to be small.

Analysis from the linearized equations further confirms this point. Given the current water depth and the stratification profile, a best performance range for the wavenumber of the long wave train is also suggested, which indicates that the weakly nonlinear models may perform better if initial wave decreases further.

6.2 Future Work

The equations used in this thesis can be generalised to model different wave effects. Some extensions are listed below.

- Given the currect initial conditions in our simulations, the Ostrovsky equation performs better than the alternative Ostrovsky equation. However, the analysis from the linearized equations suggests that the alternative Ostrovsky equation may perform better when the wavelength of the wave is very long ($\approx 160\ km$ given the current water depth and the stratification profile). More simulations with different initial conditions, for example internal tides, may be considered.
  If the alternative Ostrovsky equation can perform better than the Ostrovsky equation, we can probably consider to extend the alternative Ostrovsky equation to two dimensions. In this case, more waves can be modeled, for example Rossby waves, which needs β plane approximation.

- The water depth used in this thesis is $500\ m$. The ocean can go up to thousands of meters depth. We can increase the water depth to see the behavior of the deep water waves.

- We have only used one analytic stratification in our simulations. Other stratification profiles, including analytic and non-analytic, can be adopted.

- There are alternative equations equivalent to the weakly nonlinear equations up to $O(\epsilon^2, \mu)$, which can be derived through change of variables and aymptotic anaylsis.

Simulations from these alternative equations can be run and compared with results of the current weakly nonlinear models.

- Though we use flat bottom for all the simulations, all the codes in this thesis can be used in variable water depth as opposed to using a spectral method. In reality, the topography is more complicated and not always uniform. Different slopes can be used to see the behavior of the shoaling waves.

- Viscosity and diffusive effects can be important near the bottom boundary layer. We can add viscosity and diffusion terms to the weakly-nonlinear models and make comparisons with the fully nonlinear model.

- Only mode-one waves are tested in the numerical simulations. Waves of other mode numbers can be considered as initializations as well.

Bibliography

[1] Newell AC. *Solitons in Mathematics and Physics*. Philadelphia: Society for Industrial and Applied Mathematics, 1985. 4

[2] Liu AK, Holbrook JR, and Apel JR. Nonlinear internal wave evolution in the sulu sea. *J. Phys. Oceanogr.*, 15(12):1613–1624, 1985.

[3] John R Apel. Oceanic internal waves and solitons. *An Atlas of Oceanic Internal Solitary Waves*, 2002.

[4] Wallace AR. The malay archipelago. *Dover Publications, New York*, pages 370–374, 1869.

[5] Turkington B, Eydeland A, and Wang S. A computational method for solitary internal waves in a continuously stratified fluid. *Stud. Appl. Maths*, 85:93–127, 1991. 44

[6] Kadomtsev BB and Petviashvili VI. On the stability of solitary waves in weakly dispersing media. *Sov. Phys. Dokl.*, 15:539–41, 1970.

[7] Garrett C and Munk W. Internal waves in the ocean. *Rev. Fluid Mech.*, 11:339–369, 1979.

[8] Koop CG and Butler C. An investigation of internal solitary waves in a two-fluid system. *J. Fluid Mech.*, 112:225–51, 1981.

[9] Halpern D. Observations of short period internal waves in massachusetts bay. *J. Mar. Res.*, 29:116–32, 1971.

[10] Spiegel EA and Veronis G. On the boussinesq approximation for a compressible fluid. *Astrophysical Journal*, 131:442–447, 1960. 7

[11] Morozov EG. Oceanic internal waves (in russian). *Nauka, Moscow*, 1985.

[12] Johnson ER and Grimshaw RHJ. The reduced modified ostrovsky equation: integrability and breaking. *Physics Review E*, 2013.

[13] Michallet H and Barthelemy E. Experimental study of interfacial solitary waves. *J. Fluid Mech.*, 366:159–77, 1998.

[14] Ono H. Algebraic solitary waves in stratified fluids. *J. Phys. Soc. Jpn*, 39:1082–91, 1975.

[15] Segur H and Hammack JL. Soliton models of long internal waves. *J. Fluid Mech.*, 118:285–304, 1982.

[16] K. R. Helfrich and W. K. Melville. Long nonlinear internal waves. *Annual Review Fluid Mech.*, 38:395–425, 2006.

[17] Kar R. Helfrich and W. Kendall Melville. Long nonlinear internal waves. *Annu. Rev. Fluid Mech.*, 38:395–425, 2006. 5

[18] Karl R Helfrich. Decay and return of internal solitary waves with rotation. *Physics of fluids*, 19, 2007.

[19] P. E. Holloway, E. N. Pelinovsky, and T. G. Talipova. A generalized korteweg-de vries model of internal tide transformation in the coastal zone. *J. Geophys. Res..*, 104:18333–18350, 1999. 30

[20] P. E. Holloway, E. N. Pelinovsky, T. G. Talipova, and B. Barnes. A non-linear model of internal tide transformation on the australian north-west shelf. *J. Phys. Oceanogr.*, 27:871–896, 1997. 27, 30

[21] Grue J, Jensen A, Rusas P-O, and Sveen JK. Breaking and broadening of internal solitary waves. *F. Fluid Mech.*, 413:181–217, 2000.

[22] Grue J, Jensen A, Rusas PO, and Sveen JK. Properties of large-amplitude internal waves. *J. Fluid Mech.*, 380:257–78, 1999.

[23] Small J. A nonlinear model of the shoaling and refraction of interfacial solitary waves in the ocean. part i: Development of the model and investigations of the shoaling effect. *Journal of Physical Oceanography*, 19:755–722, 2001. 28

[24] Small J. A nonlinear model of the shoaling and refraction of interfacial solitary waves in the ocean. part i: Development of the model and investigations of the shoaling effect. *Journal of Physical Oceanography*, 19:755–772, 2001. 53

[25] Ziegenbein J. Short internal waves in the strait of gibraltar. *Deep Sea Res.*, 16:479–87, 1969.

[26] Ziegenbein J. Spatial observations of short internal waves in the strait of gibraltar. *Deep Sea Res.*, 17:867–75, 1970.

[27] Christopher R Jackson, Jose CB Da Silva, and Gus Jeans. The generation of nonlinear internal waves. *Oceanography*, 25:109–124, 2012. 2

[28] Apel JR, Proni JR, Byrne HM, and Sellers RL. Near-simultaneous observations of intermittent internal waves on the continental shelf froom ship and aircraft. *Geophys. Res. Letts.*, 2:128–131, 1975a.

[29] Russell JS. Report to committee on waves. *Report of the 7th Meeting of British Association for the Advancement of Science, London, John Murray*, pages 417–496, 1838.

[30] Russell JS. Report on waves. *Report of the 7th Meeting of British Association for the Advancement of Science, London, John Murray*, pages 311–390, 1844.

[31] Miles JW. On internal solitary waves. *Tellus*, 31:456–62, 1979. 29

[32] Hunkins K and Fliegel M. Internal undular surges in seneca lake: a natural occrurence of solitons. *J. Geophys. Res.*, 78:539–48, 1973.

[33] Lamb KG. Unpublished manuscripts. 24, 78

[34] Lamb KG. Numerical experiments of internal wave generation by strong tidal flow across a finite amplitude bank edge. *Journal of Geophysical Research*, 99:848–864, 1994. 43

[35] Lamb KG. A numerical investigation of solitary internal waves with trapped cores formed via shoaling. *F. Fluid Mech.*, 451:109–44, 2002. 43, 44

[36] Lamb KG. Shoaling solitary internal waves: on a criterion for the formation of waves with trapped cores. *F. Fluid Mech.*, 478:81–100, 2003.

[37] Lamb KG and Wan B. Conjugate flows and flat solitary waves for a continuously stratified fluid. *Phys. Fluids*, 10:2061–2079, 1998.

[38] Lamb KG and L Yan. The evolution of internal wave undular bores: comparisons of fully nonlinear numerical model with weakly nonlinear theory. *Journal of Physical Oceanography*, 26:2712–2734, 1996.

[39] Ostrovsky LA and Stepanyants YA. Do internal solitons exist in the ocean. *Rev. Geophys.*, 27:293–310, 1989. 29

[40] Ostrovsky LA and Stepanyants YA. Do internal solitons exist in the ocean? *Reviews of Geophysics*, 27:293–310, 1998.

[41] Fu LL and Holt B. Seasat views oceans and sea ice with synthetic aperture radar. *JPL Publications*, pages 81–120, 1982.

[42] RR Long. Some aspects of the flow of stratified fluids. i. a theoretical investigation. *Tellus*, 42:42–58, 1953. 14, 16

[43] Zabusky NJ and Kurskal MD. Interaction of 'solitions' in a collisionless plasma and the recurrence of initial states. *Physical Review Letters*, 15:240–243, 1965.

[44] A. R. Osborne and T. L. Burch. Internal solitons in the andaman sea. *Science*, 208:451–460, 1980. 2

[45] Choudhury R, Ivanov RI, and Liu Y. Hamiltonian formulation, nonintegrability and local bifurcations for the ostrovsky equation. *Chaos, Solitons & Fractals*, 34:544–550, 2007. 27

[46] Grimshaw R, Pelinovsky E, Talipova T, and Kurkina O. Internal solitary waves: propagation, deformation and disintegration. *Nonlin. Processes Geophys.*, 17:633–649, 2010. 27

[47] Grimshaw R, Pelinovsky E, Stepanyants Y, and Talipova T. Modelling internal solitary waves on the australian north west shelf. *Marine and Freshwater Research*, 57:265–272, 2006. 27

[48] Grimshaw R and Karl Helfrich. Long-time solutions of the ostrovsky equation. *Studies in Applied Mathematics*, 121:71–88, 2008. 3

[49] Perry RB and Schimke GR. Large amplitude internal waves observed off the northwest coast of sumatra. *J. Geophys. Res.*, 70:2319–24, 1965.

[50] Grimshaw RHJ, Karl Helfrich, and Johnson ER. The reduced ostrovsky equation: integrability and breaking. *Studies in Applied Mathematics*, 129:414–436, 2012.

[51] Grimshaw RHJ, Ostrovsky LA, Shrira VI, and Stepanyants YA. Long nonlinear surface and internal gravity waves in a rotating ocean. *Surveys in Geophysics*, 19:289–338, 1998.

[52] Joseph RI. Solitary waves in finite depth fluids. *J. Phys.*, A 10:1225–27, 1977.

[53] Pierini S. A model for the alboran sea internal solitary waves. *J. Phys. Oceanography*, 19:755–722, 1989.

[54] Thorpe SA. Asymmetry of the internal wave seiche in loch ness. *Nature*, 231:306–8, 1971.

[55] Mehrotra SC and Kelly RE. On the question of non-uniqueness of internal hydraulic jumps and drops in a two-fluid system. *Tellus*, 25:560–567, 1973.

[56] Kakutani T and Yamasaki N. Solitary waves on a two-layer fluid. *J, Phys. Soc. Jpn.*, 45:674–79, 1978. 29

[57] Kubota T, Ko DRS, and Dobbs LD. Weakly-nonlinear long internal waves in a stratified fluid of finite depth. *F. Hydronaut*, 12:157–65, 1978.

[58] Maxworthy T. Experiments on solitary internal kelvin waves. *J Fluid Mech.*, 29:365–383, 1983.

[59] Benjamin TB. Internal waves of finite amplitude and permanent form. *J. Fluid Mech.*, 25:241–270, 1966.

[60] Benjamin TB. Internal waves of permanent form in fluids of great depth. *J. Fluid Mech.*, 29:559–92, 1967.

[61] Stanton TP and Ostrovsky LA. Observations of highly nonlinear solitons over the continental shelf. *Phys. Fluids*, 14(9):2695–98, 1998. 28, 30

[62] Akylas TR and Grimshaw RHJ. Solitary internal waves with oscillatory tails. *J. Fluid Mech.*, 242:279–298, 1992. 44

[63] Chen Y and Liu PLF. The unified kadomtsev-petviashvili equation for interfacial waves. *J. Fluid Mech.*, 288:383–408, 1995.

[64] Miyatake Y, Yaguchi T, and Matsuo T. Numerical integration of the ostrovsky equation based on its geometric structures. *Journal of Computational Physics*, 231:4542–4559, 2012. 27